Developmental Biology 346 (2010) 296–309

Contents lists available at ScienceDirect

Developmental Biology

journal homepage: www.elsevier.com/developmentalbiology

Defective adult oligodendrocyte and Schwann cell development, pigment pattern, and craniofacial morphology in *puma* mutant zebrafish having an alpha tubulin mutation

Tracy A. Larson, Tiffany N. Gordon, Hiu E. Lau, David M. Parichy *

Department of Biology, Institute for Stem Cell and Regenerative Medicine, University of Washington, Box 351800, Seattle, WA 98195-1800, USA

ARTICLE INFO

Article history:
Received for publication 25 June 2010
Revised 26 July 2010
Accepted 30 July 2010
Available online 5 August 2010

Keywords:
Zebrafish
Myelination
Tubulin
Oligodendrocyte
Schwann cell
Post-embryonic development
Craniofacial skeleton
Pigment pattern

ABSTRACT

The processes of myelination remain incompletely understood but are of profound biomedical importance owing to the several dysmyelinating and demyelinating disorders known in humans. Here, we analyze the zebrafish *puma* mutant, isolated originally for pigment pattern defects limited to the adult stage. We show that *puma* mutants also have late-arising defects in Schwann cells of the peripheral nervous system, locomotor abnormalities, and sex-biased defects in adult craniofacial morphology. Using methods of positional cloning, we identify a critical genetic interval harboring two alpha tubulin loci, and we identify a chemically induced missense mutation in one of these, *tubulin alpha 8-like 3a* (*tuba8l3a*). We demonstrate *tuba8l3a* expression in the central nervous system (CNS), leading us to search for defects in the development of oligodendrocytes, the myelinating cells of the CNS. We find gross reductions in CNS myelin and oligodendrocyte numbers in adult *puma* mutants, and these deficits are apparent already during the larval-to-adult transformation. By contrast, analyses of embryos and early larvae reveal a normal complement of oligodendrocytes that nevertheless fail to localize normal amounts of *myelin basic protein* (*mbp*) mRNA in cellular processes, and fail to organize these processes as in the wild-type. This study identifies the *puma* mutant as a valuable model for studying microtubule-dependent events of myelination, as well as strategies for remyelination in the adult.

Introduction

Glia are the most abundant cells of the peripheral and central nervous systems and provide essential support and protection to neurons. The several types of glia also contribute to neuronal pathfinding, ion homeostasis, regulation of neurotransmitter release, and clearance of cellular debris, and can serve also as stem cells capable of generating a range of cell types (Nave and Trapp, 2008; Ndubaku and de Bellard, 2008). Although glia do not themselves conduct electrical impulses, conductance along axons depends critically on the myelin sheaths produced by the myelinating glia, namely, oligodendrocytes of the central nervous system (CNS) and Schwann cells of the peripheral nervous system (PNS) (Baumann and Pham-Dinh, 2001; McTigue and Tripathi, 2008; Simons and Trotter, 2007; Woodhoo and Sommer, 2008).

Oligodendrocytes and Schwann cells have distinct developmental origins. Oligodendrocytes of the spinal cord arise primarily from precursor cells at the ventral midline while oligodendrocytes of the brain arise from precursors in discrete pools both dorsally and ventrally (Ivanova et al., 2003; Kalani et al., 2008; Kessaris et al., 2006; Kim et al., 2008; Kirby et al., 2006; McTigue and Tripathi, 2008; Menn et al., 2006). By contrast, Schwann cells are derived from embryonic neural crest cells, which disperse from the dorsal neural tube and contribute to a wide range of other derivatives including pigment cells, sensory neurons, and mesenchymal cells of the craniofacial skeleton (Dutton et al., 2001; Jessen and Mirsky, 2005; Le Douarin, 1999; Lyons et al., 2005; Woodhoo and Sommer, 2008). Oligodendrocytes and Schwann cells also differ in other ways, including the simultaneous ensheathment of multiple axons by oligodendrocytes but not Schwann cells, the roles in axon guidance of Schwann cells but not oligodendrocytes, and differences in the expression or requirements for several genes encoding myelin components. Nevertheless, the most basic function of these glia–the production of a myelin sheath to support and protect axons, and to enhance electrical conductance–is a shared property of these different cell types.

While oligodendrocytes and Schwann cells present many basic questions of morphogenesis and patterning, an understanding of the establishment, maintenance, and replenishment of these cells also has profound biomedical implications, as several disorders of myelination and myelinating glia are known, and some of these occur at relatively high frequencies. In the CNS, myelination disorders include multiple sclerosis, leukodystrophies, periventricular leucomalacia, multiple system atrophy, and Pelizaeus–Merzbacher disease (Benarroch, 2009; Inoue, 2005; Nguyen et al., 2006; Wenning et al., 2008; Woodward, 2008; Zeis and Schaeren-Wiemers, 2008). Likewise, in the PNS there are several genetically distinct disorders known collectively as Charcot Marie Tooth disease or Hereditary Motor and Sensory Neuropathies (Berger et al., 2006; Scherer and Wrabetz, 2008). Whether the particular disorder is demyelinating, involving the degeneration and loss of

* Corresponding author.
E-mail address: dparichy@u.washington.edu (D.M. Parichy).

0012-1606/$ – see front matter © 2010 Elsevier Inc. All rights reserved.
doi:10.1016/j.ydbio.2010.07.035

myelin, or dysmyelinating, involving a failure of initial myelin development, and whether congenital or acquired, there is a growing interest in myelin repair and mechanisms by which remyelination might be stimulated (Chandran et al., 2008; Dubois-Dalcq et al., 2008; Franklin and Ffrench-Constant, 2008).

Animal models are a critical resource for studying myelination and remyelination therapies, and several mouse mutants have been utilized in this manner (Hardy, 1998; Readhead and Hood, 1990; Roach et al., 1985; Wenger et al., 2000). More recently, the zebrafish has been identified as an additional valuable model organism for such analyses. Many of the molecular and cellular mechanisms underlying gliogenesis and myelination are conserved in zebrafish (Buckley et al., 2008; Monk and Talbot, 2009). Moreover, recent screens for zebrafish mutants have led to the identification of genes required for glial development as well as later steps in myelin sheath formation (Dutton et al., 2001; Lyons et al., 2008, 2009, 2005; Monk et al., 2009; Pogoda et al., 2006; Voas et al., 2007; Woods et al., 2006). Most zebrafish mutants reported thus far have defects that are first apparent by the early larval period (5–7 days post-fertilization, dpf), by which time myelination has been initiated in wild-type fish. Studies of remyelination mechanisms and therapies also would be enabled by mutants with myelination defects arising principally during later development, as such phenotypes could parallel some human disorders.

In this study, we report on the zebrafish *puma* mutant, which was recovered in a screen for mutations affecting the adult pigment pattern (Parichy and Turner, 2003; Parichy et al., 2003). *puma* mutants have a normal complement of neural crest-derived embryonic and early larval pigment cells, including melanin-containing melanophores. During the larval-to-adult transformation, however, these fish develop markedly fewer "metamorphic" melanophores than the wild-type, resulting in gross perturbations to the normal pigment pattern of adult stripes. During these later stages, *puma* mutants also have a reduced complement of Schwann cells and exhibit defasciculation of peripheral nerves.

Here, we examine the onset of myelination defects in the PNS and also uncover defects in adult craniofacial morphology and swimming behavior. We then map the *puma* mutant phenotype, identify a mutation in the alpha tubulin-encoding gene *tuba8l3a*, and establish the orthology of this gene relative to other alpha tubulin loci. We show that *tuba8l3a* is expressed widely in the early embryo whereas expression becomes apparent in the CNS during the larval-to-adult transformation. This observation led us to test if PNS myelination defects are paralleled by CNS defects in oligodendrocyte specification or myelination. While early oligodendrocytes develop relatively normally, we find defects in myelin basic protein mRNA localization and a gross reduction in CNS myelination and the numbers of differentiated oligodendrocytes, both during the larval-to-adult transformation and in the adult. Together, these analyses link myelination, pigment pattern, and craniofacial defects to an alpha tubulin mutation, and identify the *puma* mutant as a potentially valuable model for future studies of myelination as well as tests of therapeutic remyelination strategies.

Materials and methods

Fish rearing, staging, genetic stocks, genetic mapping, and genotyping

Fish were reared at 28–29 °C, 14:10D. Embryonic staging followed (Kimmel et al., 1995) and post-embryonic staging used standardized standard length (SSL) measurements following (Parichy et al., 2009). The *puma*^{j115e1} allele was isolated in an early pressure gynogenetic screen for mutations induced by *N*-ethyl-*N*-nitrosourea mutagenesis in the SJD background. *puma* was subsequently introgressed into AB^{wp}, an inbred line used for genetic mapping, and map crosses were generated by crossing homozygous *puma* mutants to the inbred wik genetic background, then backcrossing the resulting F1s to *puma* mutants. A wild-type *sox10*::GFP reporter line was generously provided by R. N. Kelsh. For genotyping fish in experiments, we amplified a 944 bp product that included the *tuba8l3a* lesion (see text) and we distinguished wild-type and *puma* mutant haplotypes by differential cutting with restriction enzymes *Dde*-I, *Rsa*-I, or *Nla*-IV.

In situ hybridization

In situ hybridization followed standard procedures. For some analyses, fish were sectioned by vibratome at 200–250 μm prior to hybridization, whereas other specimens were sectioned by vibratome or cryostat following staining. Both approaches gave similar results. In situ hybridizations on embryos followed standard protocols, which were used for vibratome sections of post-embryonic specimens as well (digesting with 10 μg/ml Proteinase-K for 30 min at room temperature). Detailed methods for in situ hybridization of whole-mount post-embryonic specimens can be found at: http://protist.biology.washington.edu/dparichy/. In brief, post-embryonic fish were fixed in 4% paraformaldehyde, 1% DMSO in PBS overnight then transferred to 100% methanol at −20 °C, after which they were rehydrated, digested with 20 μg/ml Proteinase-K, 1% DMSO in PBS containing 0.1% Tween-20 (PBST) for 10–30 min at room temperature, then fixed in 4% paraformaldehyde for 20 min at room temperature, rinsed three times in PBST followed by three rinses in hybridization solution lacking yeast tRNA or heparin. Specimens were pre-hybridized in hybridization solution (50% formamide, 5× SSC, 0.5 mg/ml yeast tRNA, 0.2% Tween-20, 50 μg/ml heparin, pH 5.2 adjusted with 1 M citric acid) at 68 °C for 2 h then hybridized overnight at 68 °C with probes designed or hydrolyzed to be ~500 nucleotides in length. Specimens were then washed in 2× SSCT (SSC containing 0.2% Tween-20) twice for 10 min each, followed by washing in 0.2× SSCT twice for 30 min each, with a final wash in 2× SSCT for 2 h. All washed were done at 68 °C and specimens were transferred to plastic mesh-lined carriers and floated in large beakers with gentle agitation for 0.2× SSCT and the final 2× SSCT washes. Specimens were transferred gradually to PBST at room temperature and blocked in 5% heat-inactivated goat serum, 2 mg/ml bovine serum albumin in PBST for 2 h to overnight, then incubated in 1:5000 anti-digoxygenin Fab fragments conjugated to alkaline phosphatase (Roche) in blocking solution. After a 24-hour incubation at 4 °C with gentle agitation, specimens were transferred to mesh-lined carriers and washed for 24 h in 2 l PBST at 4 °C with gentle stirring and one change of solution during this time. Staining was performed after rinsing three times in alkaline phosphatase staining buffer using NBT and BCIP (Roche). Staining was stopped with PBS pH 5.5 after which specimens were stored in 4% paraformaldehyde. For examining in cryosections, specimens were transferred to a 15% sucrose solution then a 30% sucrose solution, embedded in OCT, and sectioned at 250 μm. For vibratome sections, larvae were embedded in 4% agarose and sectioned at 250 μm.

For in situ hybridization on frozen sections, specimens were fixed as above then sectioned in a cryostat at 25 μm, dried and rehydrated in pre-heated hybridization solution, then incubated with probe overnight at 58 °C. Slides were then washed for 1 h in 2× SSCT followed by 1 h in 0.2× SSCT in slide staining dishes at 58 °C, transferred to PBST, blocked, incubated with anti-digoxygenin Fab fragments overnight at 4 °C, washed three times in PBST for 15 min each, then incubated in alkaline phosphatase buffer and staining with NBT and BCIP. Staining was stopped as above and specimens were dehydrated through an ethanol series, cleared in xylene, and mounted with Permount.

Histochemistry and immunohistochemistry

Prior to overnight fixation in 4% paraformaldehyde, juvenile and adult heads were fixed in 4% paraformaldehyde in an ice bath and subjected to microwave fixation in a variable power Panasonic microwave with inverter technology (150 W 1 min, off 1 min repeated twice; followed by 400 W 20 s, off 20 s, repeated three times). After fixation, heads were transferred to a 15% sucrose solution followed by a

30% sucrose solution, then embedded in OCT. Cryosections of 50 μm thickness were collected on slides and air dried on a slide warmer for at least 30 min.

For staining with Black Gold II (Histochem, Jefferson AK), cryosections collected on slides were rehydrated in PBS three times for 5 min each, post-fixed in 4% PFA at room temperature for 1 h, and rinsed briefly in distilled water. The slides were then transferred to a pre-warmed solution of 0.3% Black Gold II in 0.9% NaCl at 60–65 °C for 12–18 min. Sections were rinsed in distilled water for about 2 min, followed by 3 min in 1% sodium thiosulfate, and three 5 min washes of tap water. After dehydrating on a slide warmer, sections were immersed in xylene for 1–2 min then coverslipped with Permount.

For immunohistochemistry, cryosections collected on slides were rehydrated in PBS with 0.3% Triton X-100 and post-fixed in 4% PFA at room temperature for 1 h. Slides were then transferred to water for 5 min, acetone for 7 min at −20 °C, water for 5 min at room temperature, followed by a wash in PBS with 1% Triton X-100. Sections were then incubated in blocking solution (PBS containing 10% goat serum and 0.5% Triton X-100) at room temperature for 30 min, then in rabbit antibody to MBP (1:50 diluted in block) overnight at 4 °C. This was followed by three 10-minute PBS washes and incubation with secondary antibody (1:400 diluted in block, Alexa Flour 568 goat antibody to rabbit) for 45 min at room temperature. After three 10 min washes in PBS, slides were coverslipped with anti-fade mounting medium.

For clearing and staining to reveal craniofacial bone and cartilage, fish were fixed 48 h in 4% paraformaldehyde, dehydrated, stained 24 h at room temperature in 0.02% (w/v) Alcian blue in 70% ethanol:30% acetic acid, neutralized in sodium borate solution for 12 h, bleached in 0.45% H_2O_2, 0.85% KOH, digested with 1% (w/v) trypsin in saturated sodium borate, then stained 24 h at room temperature with 0.1% (w/v) Alizarin red in 1% KOH for 24 h at room temperature. After detaining in trypsin solution, specimens were transferred to glycerol for storage (Potthoff, 1984).

Imaging and statistical analysis

Specimens were imaged with Axiovision HR or MR cameras on a Zeiss Observer inverted microscope with Apotome, a Zeiss Axioplan 2i, or an Olympus SZX-12 stereomicroscope. For thick specimens, multiple focal planes were captured using the Extended Focus or 6D Acquisition modules of Zeiss Axiovision 4.0. Images were transferred to Photoshop and adjusted for color balance when necessary. Statistical analyses were performed in JMP 8 (SAS Institute, Cary NC). *plp*+ cells were compared between sections of wild-type and *puma* mutant brains matched for anterior–posterior axial level, using a paired *t*-test. For imaging of *sox10*:GFP, larvae were fixed overnight in 4% paraformaldehyde then transferred to glycerol after which eyes were removed and specimens mounted individually between coverslips; z-stacks were collected and then deconvolved using the fast-iterative algorithm of Axiovision software.

Electron microscopy

Specimens were fixed overnight or longer in 2.5% glutaraldehyde, 1% paraformaldehyde, 2.5% DMSO in 0.05 M Pipes and then transferred to 0.1 M cacodylate/0.1 M sucrose buffer. Specimens were post-fixed 1 h at room temperature with 1% OsO_4/0.1 M cacodylate buffer, washed with distilled water and stained en bloc for 1 h at room temperature with 2% uranyl acetate. After washing, specimens were dehydrated and embedded in Spurr's Low Viscosity Epoxy Resin (Polysciences, Warrington PA). Blocks were thick sectioned at 1 μm and sections were stained with toluidine blue for orientation purposes, and then were thin sectioned at 80–100 nM, with sections mounted on grids and post-stained with 7% uranyl acetate/Reynolds lead citrate. Sections were viewed with a JEOL JEM-1200EXII transmission electron microscope at 80 kV and imaged with an Olympus-SIS Morada digital camera with iTEM software.

Phylogenetic analysis

To assess tubulin gene orthologies, inferred protein coding sequences were aligned with ClustalW, inspected by eye, then used for reconstructing phylogenetic relationships with MrBayes 3.1.2 (4×10^6 generations with sampling every 1000 generations yielding a final standard deviation of split frequencies = 0.01, default 25% burn-in, 2 runs, 4 chains, and a temperature of 0.08) (Huelsenbeck and Ronquist, 2001). Additional parsimony-based analyses were performed using protpars in the Phylip suite of phylogenetic analysis programs (Felsenstein, 1989) with 200 bootstrap replicates.

Morpholino knockdown

Knockdown of *tuba8l3a* and *dnajb2* followed standard protocols and used the following translation-blocking (tb) and splice-blocking (sb) morpholinos and corresponding mismatch controls at dosages ranging from 0.5 to 12.0 ng, with native sequences verified for all genetic backgrounds. Effects of morpholinos targeted to *tuba8l3a* were compared to effects produced using the corresponding 5 nucleotide mismatch controls and morphant phenotypes reported were not evident in embryos injected with equal doses of mismatch morpholinos. Sequences of morpholino oligonucleotides were as follows (mismatch nucleotides shown in lower case): tuba8l3a-tb1, TTGTCAGATTTCCCTTCAGGCCGAC; tuba8l3a-tb1 5 mis, TTcTCAcATTTCCgTTCAcGCCcAC; tuba8l3a-tb2, GATTCGGAAAGAGAAGGCAGATGTC; dnajb2-tb, GAACATCATAGTAGT CCACCATCGC; dnajb2-sb, CAAAGGCAGTTTCGACTTACGCTTT.

Results

Pleiotropic defects of puma mutant adult zebrafish

puma mutants are homozygous-viable and exhibit gross defects in adult pigment pattern formation with substantial reductions in the numbers of metamorphic melanophores, xanthophores and iridophores (Fig. 1A) (Parichy and Turner, 2003; Parichy et al., 2003). These fish also exhibit a variably penetrant jaw defect. Clearing and staining revealed alterations in skull shape and reduced bone density as well as mispositioning of the jaw (Figs. 1B and C). These defects were not evident in embryos and early larvae, but became apparent in juveniles and were increasingly severe as fish aged. Interestingly, male *puma* mutants were significantly more likely to exhibit these craniofacial defects than were female *puma* mutants (Fig. 1G).

puma mutant larvae are deficient for Schwann cells and have disorganized and defasciculated peripheral nerves during the larval-to-adult transformation (Parichy et al., 2003). We asked when defects in the Schwann cell lineage first arise. At 24 h post-fertilization (hpf) we found no differences in the distributions of cells expressing *sox10* (Supplementary Fig. S1) or *crestin* (data not shown), suggesting that early neural crest and Schwann cell development are unaffected. Likewise, at 5 days post-fertilization (dpf) and 7 dpf, we observed normal numbers of differentiated Schwann cells expressing *myelin basic protein* (*mbp*) along the lateral line nerve (Fig. 1D), and these cells developed myelin sheaths surrounding axons, both of which were ultrastructurally indistinguishable from the wild-type (data not shown). By contrast, we found a reduced but variable complement of Schwann cells once the larval-to-adult transformation had commenced (Fig. 1E), and still fewer Schwann cells as fish approached juvenile stages (Fig. 1F). These data indicate that Schwann cells develop normally in the embryo but disappear during the larval-to-adult transformation.

Finally, *puma* mutant juveniles and adults also display locomotor defects. We quantified these by dropping fish six inches from a net into a small tank of water. Among siblings derived from intercrosses of *puma*

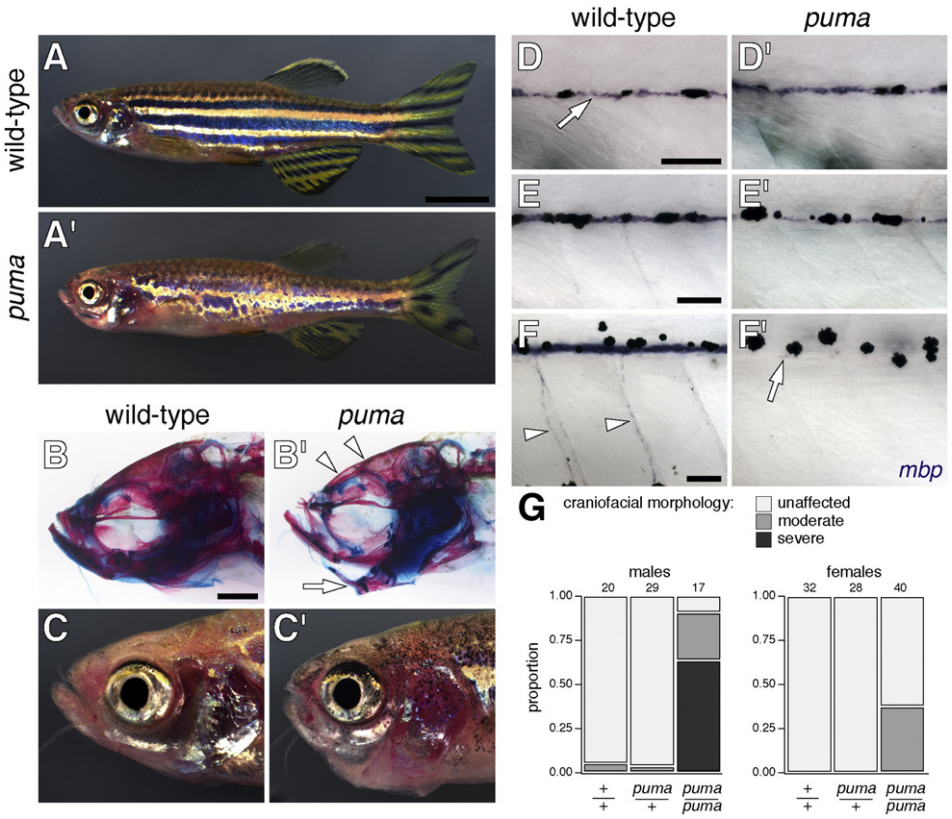

Fig. 1. *puma* mutant adult zebrafish exhibit defects in pigment pattern, craniofacial morphology, Schwann cell development, and locomotor behavior. (A, A′) Adult stripes and craniofacial morphology are disrupted in *puma* mutants. (B, B′) Clearing and staining to reveal bone (red) and cartilage (blue) shows thinner dysmorphic bones of the skull in *puma* mutants (arrowheads) and ventral displacement of the jaw (arrow). (C, C′) External anatomy of head for wild-type and a severely affected *puma* mutant. (D–F) Development of Schwann cell defects. (D, D′) Early larvae exhibit *mbp*+ Schwann cells covering the lateral line nerve (arrow) in both wild-type and *puma* mutants (here, 4.0 mm standardized standard length, 4.0 SSL). (E, E′) During later post-embryonic development, *mbp*+ cells are more sparsely arranged in *puma* mutants (here, 6.3 SSL). (F, F′) *mbp*+ cells are nearly absent in *puma* mutants, with only rare residual cells found along the lateral line (arrow in F′); *mbp*+ cells found along dorsoventrally oriented nerves in wild-type (arrowheads in F) are completely lacking in *puma* (8.0 SSL). (G) Quantitative analysis of craniofacial defects in *puma* mutants. Shown are the proportions of individuals placed into different categories for severity of craniofacial defect, divided by sex and genotype. Numbers of individuals examined are given above the bars. Contingency table analysis shows that homozygous *puma* mutants were more likely than wild-type to exhibit craniofacial defects and such defects were more prevalent among males than females (genotype: $\chi^2 = 93.0$, $P<0.0001$; sex: $\chi^2 = 43.7$, $P<0.0001$; $n = 171$). Scale bars: in A, 4 mm for A, A′. In B, 1 mm for B, B′; in D, 60 μm for D, D′; in E, 60 μm for E, E′; in F, 60 μm for F, F′.

mutant heterozygotes, wild-type individuals swam immediately, or more rarely, as soon as the bottom was touched ($n = 159$). By contrast, 26% of *puma* mutants settled motionless on the bottom for at least 2 s ($n = 65$; $X^2 = 40.4$, $P<0.0001$; Supplementary Videos 1 and 2), and, in contrast to craniofacial defects, females were three times more likely to exhibit this locomotor defect than were males ($X^2 = 5.8$, $P<0.05$).

A lesion in the alpha tubulin gene, tuba8l3a, in puma mutants

We mapped the *puma* mutant to chromosome 9 in the vicinity of *dnajb2* (*zgc:153268*), and between microsatellite markers z34459 and z3124. Using a partial genomic assembly from shotgun sequence data, we developed additional markers including NW634218f1, for which we found no recombinants with the *puma* mutant phenotype in 4402 meioses. To narrow and refine the critical genetic interval, we identified five genomic PAC clones containing the NW634218f1 target sequence. Sequencing two of these clones (53A17 and 257H5) and genetically mapping additional markers revealed a critical interval of ~46 kb containing two open reading frames predicted to encode alpha tubulins, one of which corresponded to *tubulin alpha 8-like 3* (*tuba8l3*), identified previously as an expressed sequence tag in the zebrafish gene collection (*zgc:101117*; fc51h10.x1), and here designated *tuba8l3a* (Fig. 2A; GenBank Accession GU131676). The second locus, here designated *tuba8l3b* (GenBank Accession GU131677), was 92% identical to *tuba8l3a* within the aligned open reading frame and produced transcript detectable by PCR (data not shown). Nevertheless, the open reading frame also included an insert of 81 nucleotides encoding 27 amino acids dissimilar to other tubulins, raising the possibility that *tuba8l3b* is an expressed pseudogene.

We searched for ENU-induced mutations in *tuba8l3* and *tuba8l3b* by sequencing genomic DNA from *puma* mutants and comparing to wild-type stocks. We identified a single T→A transversion in the *puma* mutant allele of *tuba8l3a* at position 747 of the open reading frame, resulting in a non-conservative amino acid substitution at residue 249 of the predicted protein, exchanging asn (uncharged) for lys (basic) (Fig. 2B). T747A introduces a *Dde*-I restriction site into the *puma* mutant allele and eliminates an *Rsa*-I restriction site present in the wild-type allele; these restriction fragment length polymorphisms segregated with the *puma* mutant phenotype (0 recombinants in 4402 meioses).

Comparison of the *puma* mutant *tuba8l3a* allele to wild-type *tuba8l3a* alleles supports the inference that T747A is an ENU-induced mutation. In addition to T747A, we found 21 silent nucleotide differences between the *puma* allele and the inbred, wild-type allele of AB^{wp}, into which *puma* was introgressed prior to mapping; each of these was shared, however, between *puma* and the wild-type, pre-mutagenized allele of SJD, from which *puma* was derived (Fig. 3C). Thus, T747A was the only unique substitution found in the mutagenized *puma* allele. *puma*/SJD nucleotide variants in the 3′ half of the open reading frame also were shared with *tuba8l3b*, suggesting an ancestral episode of gene conversion between these neighboring loci.

To assess the potential functional significance of asn249lys, we compared the inferred *puma* mutant protein to other tubulins. The wild-type asn at this position is conserved in at least 89 other alpha-tubulins,

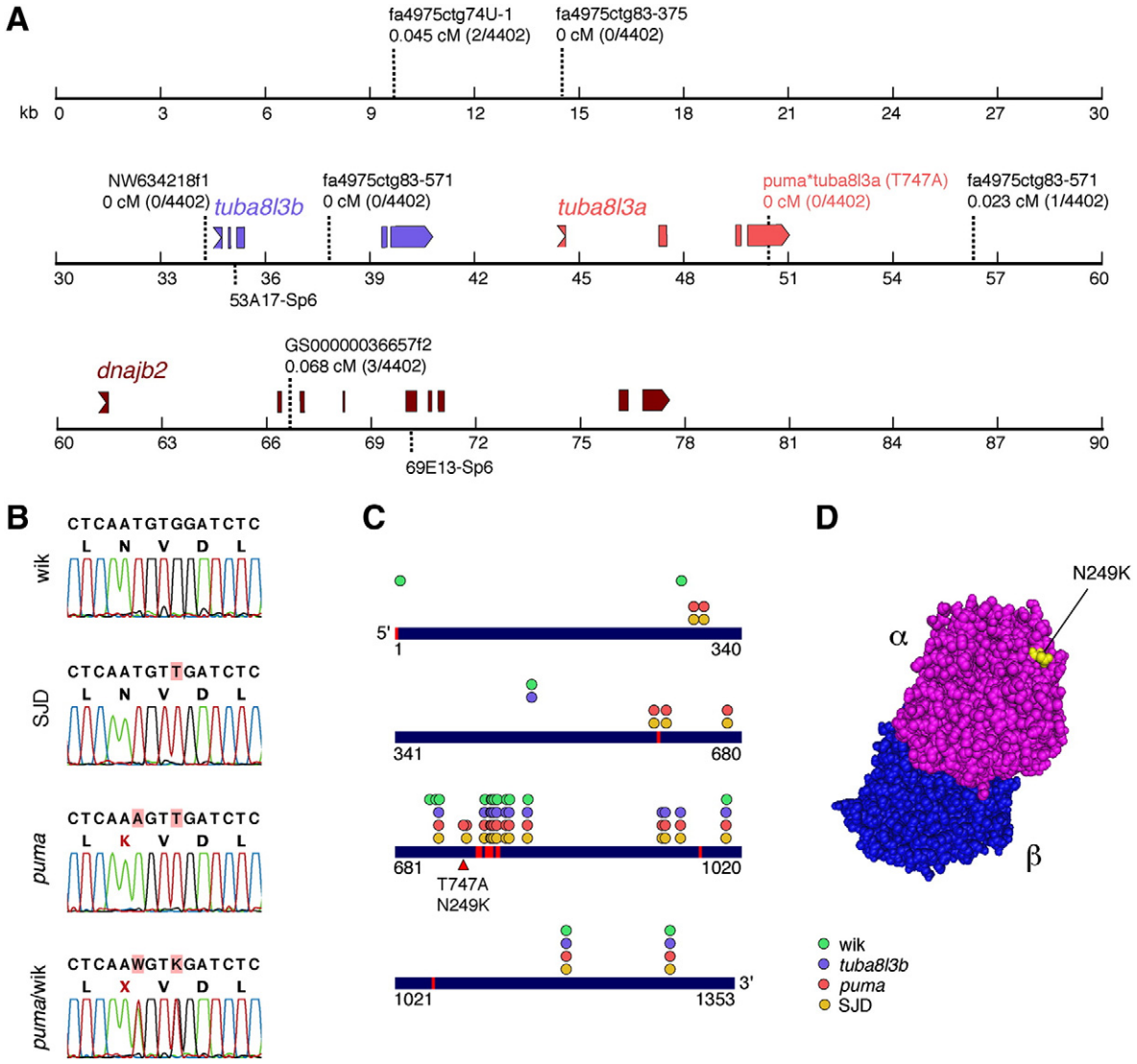

Fig. 2. Identification of an alpha tubulin lesion in the *puma* mutant. (A) Critical genetic and physical interval for the *puma* mutant locus. Genetic markers and their associated genetic distances are shown above the horizontal scale; PAC end sequences in this region are shown below the horizontal scale. (B) Electropherograms for *tuba8l3a* showing single nucleotide polymorphism between genetic backgrounds and lesion present in *puma* mutant (nucleotides highlighted with pink). Top to bottom: wild-type wik sequence; wild-type SJD with silent G→T transversion; homozygous *puma* mutant illustrating SNP shared with SJD and novel T→A transversion, resulting in a non-conservative N→K substitution; *puma*/+ map-cross individual heterozygous for both polymorphic sites. (C) Schematic of the *tuba8l3a* cDNA indicating unique and shared polymorphisms between strains. Only the *puma* haplotype exhibits the T747A substitution. Red, beta/alpha domain interface. (D) N249K substitution mapped onto structural model of an αβ-tubulin dimer (Nogales et al., 1998b) (MMDB ID: 8900, PDB ID: 1TUB).

beta-tubulins, and gamma-tubulins in *Saccharomyces*, *Arabidopsis*, *Drosophila*, and vertebrates, as well as in the *E. coli* tubulin-like cell division protein, ftsZ (Nogales et al., 1998a) (an exception is the divergent *Drosophila melanogaster* tubulin *CG77947* and its orthologues in other *Drosophila* species, which exhibit a conservative change from asn to thr). Moreover, asn249lys occurs at the surface of the alpha tubulin monomer adjacent to an element of the beta/alpha domain interface, which is essential for the polymerization of alpha/beta tubulin dimers during microtubule assembly (Fig. 3D) (Downing and Nogales, 1999; Lowe et al., 2001). We did not find gross defects in *tuba8l3a* transcript abundance in *puma* mutants (data not shown) raising the possibility that the mutant tubulin exerts an antimorphic effect. Consistent with this notion, we were unable to isolate new alleles even after extensive non-complementation screening (and see below).

Finally, we also considered the possibility of a lesion in *dnajb2*. Although its coding sequence lies outside of the critical genetic interval, *cis* regulatory elements might be found within this interval: mutations in such elements might lead to alterations in *dnaj2b* expression and could, conceivably, be responsible for the *puma* mutant phenotypes (Fig. 2A). We were unable to detect *dnajb2* expression by in situ hybridization at embryonic or post-embryonic stages, quantitative RT-PCR did not reveal differences in *dnajb2* expression between wild-type and *puma* mutants, there were no detectable alterations in splicing or induced mutations in the open reading frame of *puma dnajb2* as compared to the ancestral SJD haplotype, and neither splice-blocking nor translation-blocking morpholinos phenocopied an early larval *puma* mutant defect (see below). These analyses likely exclude allelism of *dnajb2* and *puma*. By contrast, the correspondence of *tuba8l3a* to *puma* is strongly suggested by the presence of a presumptively ENU-induced lesion that segregates with the *puma* phenotype and is likely to be of functional significance to microtubule assembly, stability, or both. This conclusion is further supported by analyses of *tuba8l3a* morphant early larvae below.

Orthology of tuba8l3a with other tubulin genes

Several alpha and beta tubulin genes have been implicated in neurological disorders, including lissencephaly, pachygyria, and

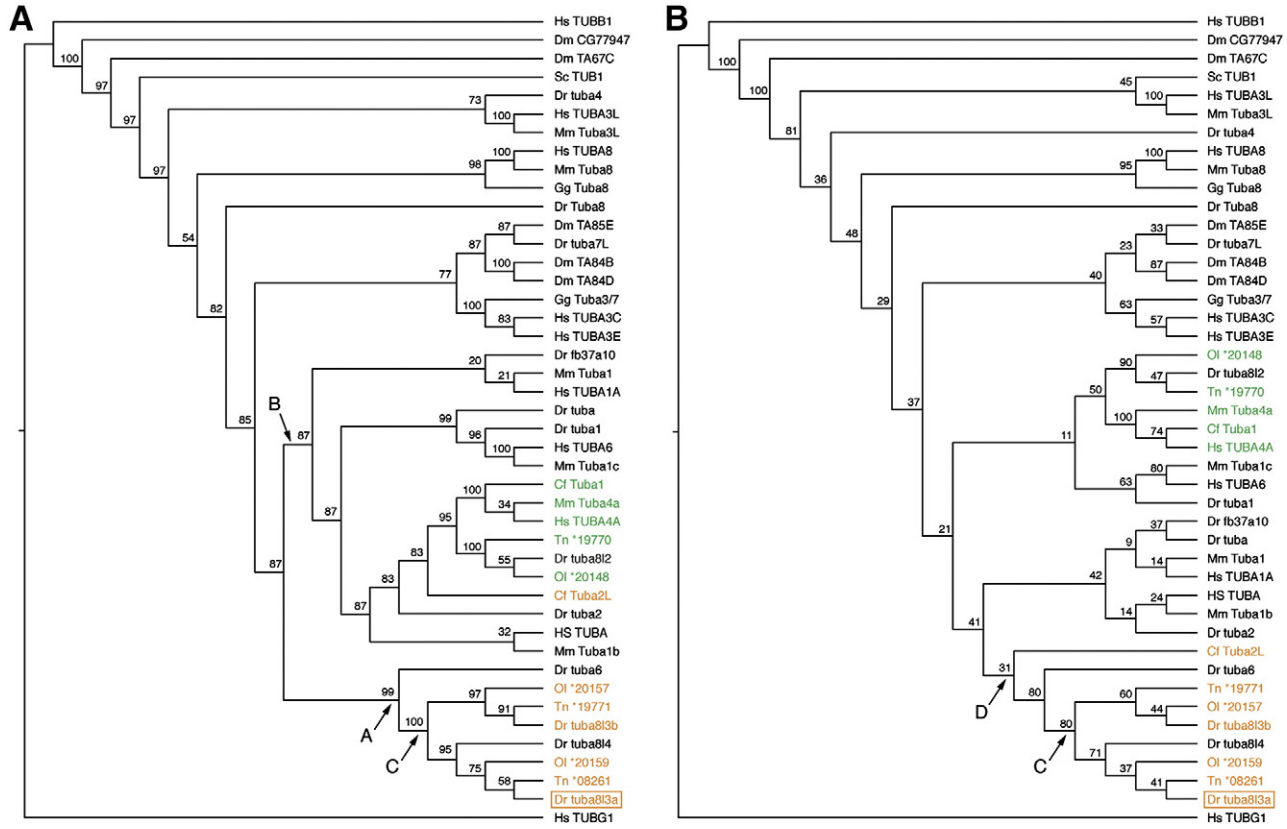

Fig. 3. Orthology of *tuba8l3a* relative to other alpha tubulin genes. (A) Bayesian phylogeny with clade credibility values for each node. (B). Parsimony phylogeny with bootstrap support for each node. Zebrafish *tuba8l3a* (*puma*) is boxed; protein colors correspond to synteny comparison in Fig. 4. See text for details. Species identifiers: Cf, *Canis familiaris*, Dm, *D. melanogaster*; Dr, *Danio rerio*; Gg, *Gallus gallus*; Hs, *Homo sapiens*; Mm, *Mus musculus*; Ol, *Oryzias latipes* (medaka); Sc, *Saccharomyces cerevisiae*; Tn, *Tetraodon T. nigroviridis* (pufferfish). Protein identifiers (Genbank) or transcript identifiers (Ensembl): Cf Tuba1, XM_858678; Cf Tuba2L, XM_848175; Dm CG7794, NP_650674.1; Dm TA67C, NP_524009.2; Dm TA84B, NP_476772.1; Dm TA84D, NP_524264.1; Dm TA85E, NP_524297.1; Dr tuba, NP_001098596.1; Dr tuba1, NP_919369.1; Dr tuba2, NP_998195.1; Dr tuba4, NP_956089.1; Dr tuba6, XP_001334783.1; Dr tuba7L, NP_001002230.1; Dr tuba8, NP_997937.1; Dr tuba8l2, NP_956985.1; Dr tuba8l3a (*puma*); Dr tuba8l3b; Dr tuba8l4, NP_956479.1; Dr WU: fb37a10, XP_688383.1; Gg Tuba3/7, XP_422851.1; Gg Tuba8, NP_990775.1; Hs TUBA, NP_006073.2; Hs TUBA1A, NP_006000.2; Hs TUBA3C, NP_005992.1; Hs TUBA3E, NP_997195.1; Hs TUBA3L, NP_079079.1; Hs TUBA4A, NP_005991.1; Hs TUBA6, NP_116093.1; Hs TUBA8, NP_061816.1; Hs TUBB1, NP_110400.1; Hs TUBG1, NP_001061.2; Mm Tuba1, NP_035783.1; Mm Tuba1b, NP_035784.1; Mm Tuba1c, NP_033474.1; Mm Tuba3L, NP_001029051.2; Mm Tuba4, NP_033473.1; Mm Tuba8, NP_059075.1; Ol *20148, ENSORLT00000020148; Ol *20157, ENSORLT00000020157; Ol *20159, ENSORLT00000020159; Sc TUB1, NP_013625; Tn *19770, ENSTNIT00000019770; Tn *19771, ENSTNIT00000019771; Tn *08261, ENSTNIT00000008261.

polymicrogyria (Jaglin et al., 2009; Keays et al., 2007; Poirier et al., 2007; Tian et al., 2008). We therefore asked whether *tuba8l3a* is orthologous to known disease genes in human. A Bayesian-based phylogeny of inferred protein coding sequences (Fig. 3A) revealed a strongly supported clade ("A") comprising zebrafish *tuba8l3a* and *tuba8l3b*, homologues of medaka fish, *Oryzias latipes*, and pufferfish, *Tetraodon nigroviridis*, as well as zebrafish tuba8l4 and tuba6. This clade excluded mammalian and avian tubulins, suggesting a teleost-specific evolutionary radiation of these loci. A sister clade ("B"), includes several tubulins of both mammals and teleosts, and does not unambiguously resolve the orthology of *tuba8l3a*.

To further evaluate the homology of *tuba8l3a* to other tubulins, we examined gene–order relationships (Fig. 4). Genetic mapping and sequencing revealed in zebrafish the linked loci *tuba8l3b*, *tuba8l3a*, *dnajb2*, *ptprn*. In the teleosts *Tetraodon* and *Oryzias* a conserved synteny group was found with these loci and as well as a third tubulin locus present on the opposite strand. Our analyses and available sequence data did not resolve whether a third, opposite strand tubulin is present in zebrafish as well. Comparisons of gene order and orientation with mammals suggested that *tuba8l3a* and *tuba8l3b* in teleosts arose from a single ancestral locus. This gene has been retained in *Canis* (*Tuba2L*), but is a known pseudogene in human (*ψTUBA4B*) and has been lost from *Mus* (Khodiyar et al., 2007). The third, opposite-strand tubulin in teleosts occurs in all three mammalian genomes (*TUBA4A* in human). A more ancient tandem duplication presumably gave rise to *TUBA4A* and *ψTUBA4B* paralogues. The Bayesian phylogeny in Fig. 3A supports these inferences for the teleost tubulins (clade "C") but not for the orthologies relative to mammalian tubulins (*ψTUBA4B* could not be included owing to its high level of divergence).

To further investigate these differences, we also performed a parsimony-based phylogenetic analysis (Fig. 3B). Despite very low bootstrap support for many clades, this inferred phylogeny was consistent with a teleost-specific tandem duplication, giving rise to *tuba8l3a* and *tuba8l3b* (clade "C"), as well as the orthology of these genes to *Canis Tuba2L* (clade "D"). Overall, these data suggest that *tuba8l3a* is orthologous to *Canis Tuba2L* and human *ψTUBA4B*, and more distantly homologous to human *TUBA4A*, which has yet to be implicated in human disease.

tuba8l3a expression in the embryo and in the larval central nervous system

To examine *tuba8l3a* expression, we were unable to use riboprobes targeted to the coding sequence owing to the high similarity with *tuba8l3b* and other tubulins more generally. We therefore designed riboprobes to recognize 60 nucleotide (nt) and 133 nt regions of the unique 5′ and 3′ untranslated regions, respectively. Both probes yielded equivalent expression patterns. In embryos, *tuba8l3a* transcripts were abundant but not spatially localized through 24 h post-fertilization (hpf; Fig. 5A); expression diminished gradually thereafter and became undetectable by 48 hpf.

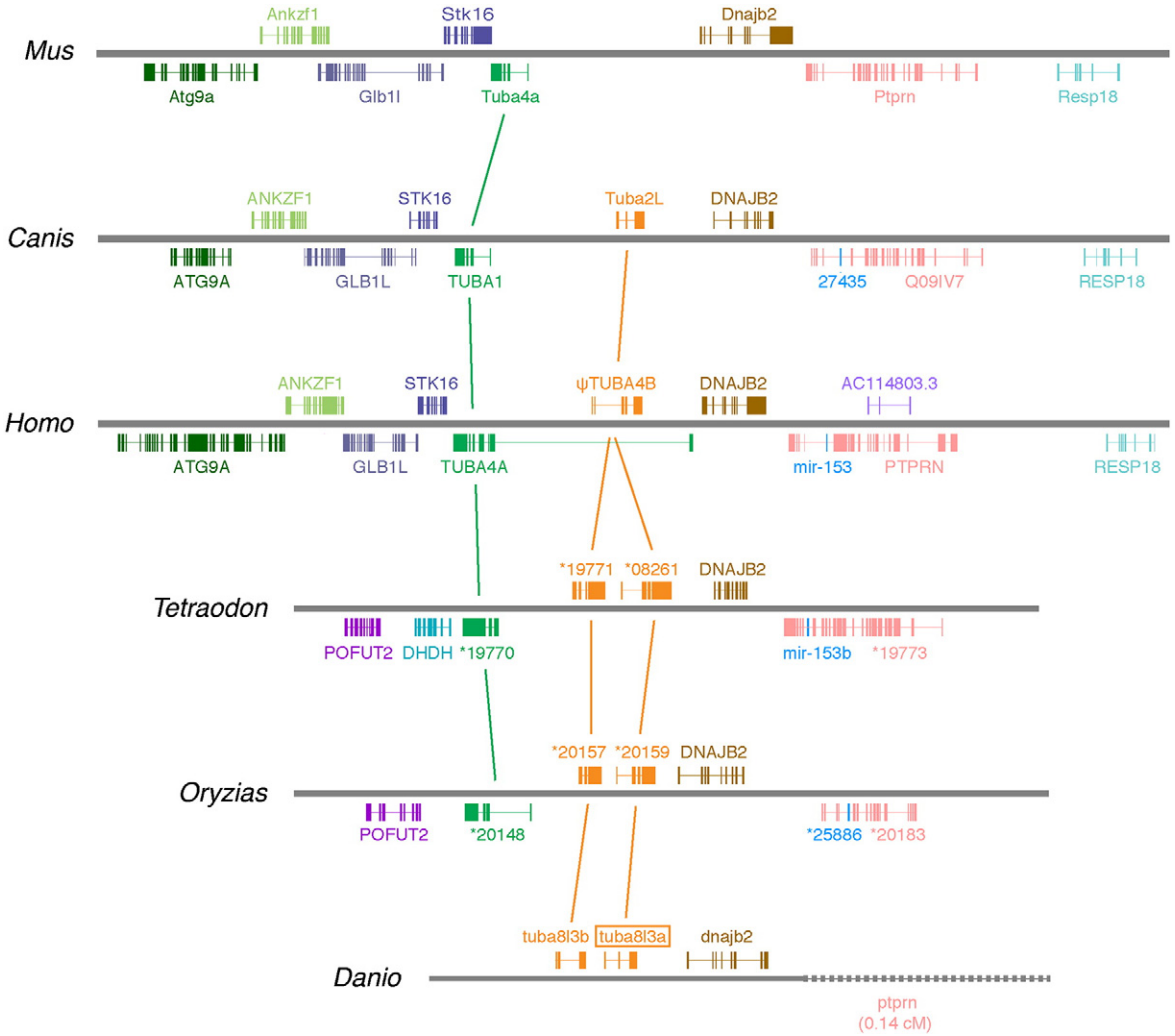

Fig. 4. Synteny analyses reveal *tuba8l3a* orthology. Shown are loci inferred to be orthologues by comparison of conserved synteny across vertebrate genomes based on Ensembl genome assemblies. *tuba8l3a* is orthologous to the human pseudogene *ψTUBA4B* and dog *Tuba2L*. Regions are not to scale. For *Tetraodon* and *Oryzias*, unnamed tubulins are indicated by transcript identifiers where the preceding "*" indicates "ENSTNIT000000" and "ENSORLT000000", respectively.

During post-embryonic development, we found *tuba8l3a* transcript in the brain and cranial ganglia (Figs. 5B and C). Transverse sections through the head revealed expression in the periventricular grey zone of the optic tectum, cranial ganglia, and the inner nuclear layer of the retina (Figs. 5D–H). Owing to the small sizes and limited sensitivities of the riboprobes we used, additional domains of expression may have escaped detection.

puma mutant adults are deficient for central nervous system myelination

Expression of *tuba8l3a* in the brain during post-embryonic development, and the locomotor defect of *puma* mutant adults, led us to examine the brains of juvenile and adult fish. *puma* mutant adult brains were less opaque than wild-type adult brains, suggesting an underlying structural difference (Fig. 6A). Although alpha tubulin mutations in human and mouse are associated with abnormal neuronal migration, lissencephaly and other disorders (Keays et al., 2007; Poirier et al., 2007), histological comparisons did not reveal gross defects in brain layering or organization in *puma* (data not shown).

By contrast, several lines of evidence indicated that *puma* mutants are deficient for brain myelination. Using Black Gold II histochemistry (Schmued et al., 2008), we found reduced staining for myelin in *puma* mutants compared to wild-type, with differences particularly apparent both in central regions of the brain and in a reduced frequency of radially oriented fibers more peripherally (Fig. 6B). An antiserum against zebrafish myelin basic protein (*mbp*) likewise exhibited reduced staining in *puma* mutants than in wild-type (Fig. 6C) (Lyons et al., 2009; Voas et al., 2007). Although female *puma* mutants were more likely to exhibit locomotor defects than male *puma* mutants, we did not detect gross differences in the severity of myelin deficiencies between sexes.

To examine the distribution of oligodendrocytes, we used the markers *mbp* and *proteolipid protein* (*plp*/*DM20*). *mbp* mRNA is localized to cell bodies as well as cellular processes, whereas *plp* mRNA is localized to cell bodies (Carson et al., 1997; Lyons et al., 2009). Juvenile *puma* mutants (4 wk, 13 SSL) had dramatically fewer *mbp*+ or *plp*+ cells than juvenile wild-type (Figs. 6D and F). During later adult development (10 wk, 24 SSL), *mbp*+ and *plp*+ cells were more frequently observed in *puma* mutants, but were still far fewer than in the wild-type (Figs. 6E and G). Transmission electron microscopy of adult fish confirmed that *puma* mutants exhibit fewer myelinated axon tracts in the central nervous system, though myelin sheaths that were present in *puma* mutants were indistinguishable from wild-type (Fig. 7). Thus, *puma* mutants have defects not only in Schwann cells but oligodendrocytes as well.

Embryonic and post-embryonic defects in oligodendrocyte development presage adult myelin defects in puma mutants

Defects in *puma* mutants could result from a demyelination in the juvenile or adult, or dysmyelination arising at earlier stages. To

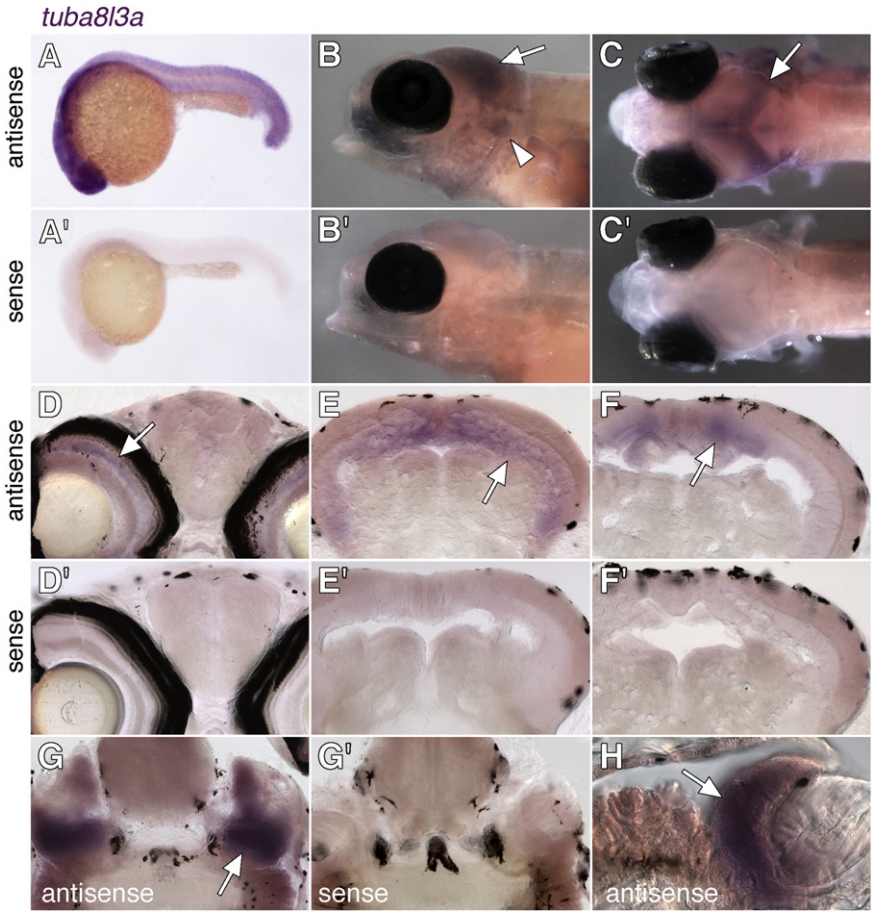

Fig. 5. *tuba8l3a* is not spatially restricted in the embryo but is expressed most prominently in the central nervous system during post-embryonic development. Shown is staining with antisense and sense probes (diluted to equal concentrations) targeted to the 5′ untranslated region of *tuba8l3a*, (A, A′) Widespread expression of *tuba8l3a* at 24 hpf. (B, B′) Lateral views of larvae (7.2 SSL) showing *tuba8l3a* transcript in the brain (arrow) and cranial ganglia (arrowhead). (C, C′) Dorsal views of the same individuals, illustrating *tuba8l3a* mRNA in the brain (arrow). Larvae in B–C are homozygous *nacre* mutants that lack otherwise obscuring melanophores due to an autonomously acting mutation in the *mitfa* transcription factor. Expression in wild-type larvae was indistinguishable from *nacre* mutants (not shown). (D, D′) *tuba8l3a* transcript is detectable in the inner nuclear layer of the retina (arrow). (E, E′, F, F′) More posteriorly, *tuba8l3a* is expressed in the periventricular grey zone of optic tectum. (G, G′, H) *tuba8l3a* staining (arrow) in the cranial ganglia. Larvae in D–H are 8–9 SSL.

distinguish between these possibilities, we determined when defects in oligodendrocyte development were first manifested by examining larvae and embryos. During the larval-to-adult transformation, we found a marked reduction in *plp*+ and *mbp*+ oligodendrocytes (Figs. 8A–E). To quantify this difference we counted the numbers of *plp*+ cells in corresponding regions of wild-type and *puma* mutant larvae. Overall, *puma* mutants exhibited only 12% as many *plp*+ cells as wild-type (means ± SE: wt, 153 ± 20; *puma*, 18 ± 4; matched $t_{11} = 6.4$, $P < 0.0001$) and residual cells typically also exhibited reduced staining for *plp*. Nevertheless, we observed similar numbers of *olig1*+ cells suggesting normal specification of the oligodendrocyte lineage at these stages (Figs. 8F and G). Myelination defects in the juvenile and adult are thus presaged by a dysmyelinating phenotype already evident during larval development.

To ascertain whether defects might be present in the earliest-arising oligodendrocytes, we examined embryos and early larvae (≤5 dpf). We found similar distributions of cells expressing *sox10* or *olig1* within the central nervous system, suggesting that *puma* mutants do not have defects in early oligodendrocyte specification or differentiation (Figs. 9A and B and data not shown). Likewise, cells expressing the later markers of differentiation *plp*, *myelin associated glycoprotein* (*mag*), and *myelin protein zero* (*mpz*), were similarly distributed between genotypes (Figs. 9D and E and data not shown). By contrast, we observed a clear difference in the pattern of *mbp* staining at these early stages (Figs. 9F and G). In the wild-type, *mbp* transcript was found in two compact tracts within the brain by 5 dpf, and relatively little mRNA was observed elsewhere in the brain. In the *puma* mutant, however, *mbp* transcript was found in cell bodies further dorsally and ventrally from the tracts observed in wild-type. This mis-patterning was not accompanied by detectably greater levels of cell death as revealed by acridine orange staining (data not shown). These differences between genotypes were similar but of lesser magnitude in 4 dpf larvae as well.

Identification of an early larval defect in *puma* mutants presented an opportunity to further test the correspondence of *tuba8l3a* to *puma* using morpholino oligonucleotides to knockdown *tuba8l3a* expression. If the *tuba8l3a* mutation is hypomorphic, then its knockdown in wild-type might phenocopy the *puma* mutant. Conversely, if the *tuba8l3a* mutation is antimorphic, then its knockdown in *puma* mutants might restore a wild-type phenotype. Injecting either of two translation-blocking morpholinos at a range of concentrations into wild-type embryos failed to fully phenocopy the *puma* 5 dpf *mbp* pattern defect, though minor perturbations were evident in ~50% of injected larvae (Figs. 9H and I); morphants did not exhibit other unique phenotypes relative to mismatch controls injected with corresponding dosages. By contrast, injection of morpholinos into *puma* mutants resulted in *mbp* staining much more similar to that of the wild-type at 5 dpf, with increased staining of processes and reduced staining of cell bodies (Fig. 9H) as compared to sibling uninjected embryos stained for equal times (Fig. 9I). Such rescues were observed in ~75% of embryos injected with 0.5 ng tuba8l3a-TB1 and ~25% of embryos injected with 1.0 ng tuba8l3a-TB2 in multiple experiments conducted over several weeks ($n = 123$ larvae imaged; >600 larvae examined). These data further support the conclusion that *puma* and

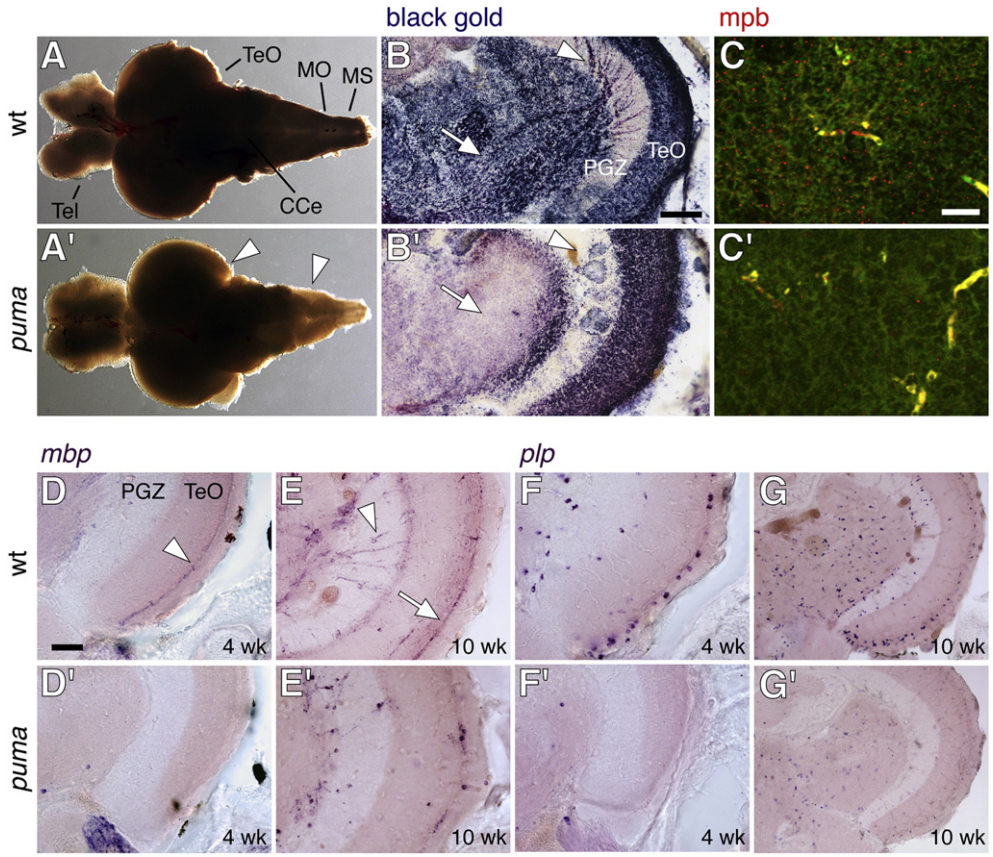

Fig. 6. Deficient central nervous system myelination in *puma* mutant adults and juveniles. (A, A′) Decreased opacity of adult brain from *puma* as compared to wild-type; this difference is especially notable at the lateral edges and posteriorly (arrowheads). Anterior to the left. Tel, telencephalon; TeO, tegmentum opticum; CCe, corpus cerebelli; MO, medulla oblongata; MS, medulla spinalis. (B, B′) Black Gold II staining for myelin in transverse sections of wild-type and *puma* mutant adults. Myelin is stained blue-black whereas other tissue is purple-red. Reduced staining in *puma* is evident to some degree within the optic tectum (TeO) but is more pronounced in ventral–medial regions (arrow), internal to the periventricular grey zone (PGZ). Radially oriented black gold staining (arrowhead) also is largely absent from the PGZ itself of the *puma* mutant. (C, C′) Antiserum against zebrafish *mbp* (red) stains numerous punctate foci in the ventral–medial brain of wild-type but far fewer in the corresponding region of *puma* mutants. Green, background tissue fluorescence. Yellow, fluorescence of blood vessels in green and red channels. (D, D′–G′, G) In situ hybridization for *mbp* and *plp* in juveniles and adults (13 SSL, 24 SSL). (D, D′) In juveniles, staining for *mbp* is pronounced in a band (arrowhead) near the outer surface of the optic tectum (TeO) in wild-type (D) but is not apparent in *puma* (D′). (E, E′) In adults, abundant *mbp* transcripts are found radially in the PGZ (arrowhead) and at the outer surface of the optic tectum (arrow) in wild-type but are found at lower levels in *puma*. (F, F′) In juveniles, *plp* staining is detected in individual cell bodies both interiorly (arrowhead) and near the tectum surface (arrow) of wild-type but there are far fewer of these cells in *puma* mutants. (G, G′) In adults, numerous *plp*-expressing cell bodies are observed in wild-type, whereas in *puma* mutants there are fewer cells and those present are less densely stained. Scale bars: in B, 100 μm; in C, 20 μm; in D, 100 μm for D–G.

tuba8l3a are allelic and suggest both a role for native *tuba8l3a* in oligodendrocyte development, as well as an antimorphic effect of *puma* mutant tuba8l3a on microtubule function.

Because *mbp* mRNA localizes to oligodendrocyte processes (Carson et al., 1997; Lyons et al., 2009), mis-patterning in *puma* mutants could reflect a failure by oligodendrocytes to extend processes or a failure of *mbp* mRNA transport within these processes. To distinguish between these possibilities, we examined whether oligodendrocytes extended processes by 5 dpf. We crossed *puma* mutants to a *sox10*::GFP reporter line that marks oligodendrocytes (Kirby et al., 2006), then backcrossed the resulting progeny to generate GFP+ embryos segregating the *puma* mutant phenotype. We imaged native GFP expression in each fish, then genotyped each individual by RT-PCR ($n=82$ larvae). Oligodendrocyte processes were apparent in both wild-type and *puma* mutants (Figs. 10A–C), demonstrating that mutant cells are capable of process extension. Yet, these analyses also revealed a defect in process organization. In wild-type, most GFP+ processes in the region examined were oriented anteroposteriorly and formed relatively compact dorsal and ventral tracts. In *puma* mutants, however, processes were frequently oriented away from the anterior–posterior axis and failed to form the compact tracts observed in wild-type. Together, these data indicate that although *puma* mutant oligodendrocytes form processes, these cells fail to properly localize *mbp* mRNA in these processes, and also exhibit defects in process organization with resulting defects in early myelination.

Finally, we considered the possibility that the *tuba8l3a* lesion could result in compensatory or other alterations in cytoskeletal modifying proteins. For example, *silent information regulator 2* (*sirt2*) co-localizes with microtubules, acts as an alpha tubulin deactetylase, and retards oligodendrocyte arborization and terminal differentiation (Li et al., 2007; North et al., 2003), whereas 2′,3′-cyclic nucleotide 3′-phosphodiesterase (CNP) binds to tubulin heterodimers and promotes microtubule assembly as well as oligodendrocyte arborization and terminal differentiation (Lee et al., 2005). We did not find differences between wild-type and *puma* mutants in either *sirt2* or *CNP* expression (e.g., Fig. 8H and data not shown). Likewise, we were unable to detect differences between genotypes for additional markers of central nervous system organization, progenitor zones, or other glial lineages during embryonic or post-embryonic stages [e.g., *reelin*, *disrupted in schizophrenia* (*disc1*), *nkx2.2*, *glial fibrillary acidic protein* (*gfap*), *her5*, *atoh1a*; Figs. 9 8H–J and data not shown].

Discussion

We showed that zebrafish *puma* mutants exhibit profound defects in myelination of the adult CNS and PNS, as well as locomotor abnormalities and dysmorphic patterning of the craniofacial skeleton. These mutant phenotypes are in addition to a failure of adult pigment pattern development, described previously (Parichy and Turner, 2003;

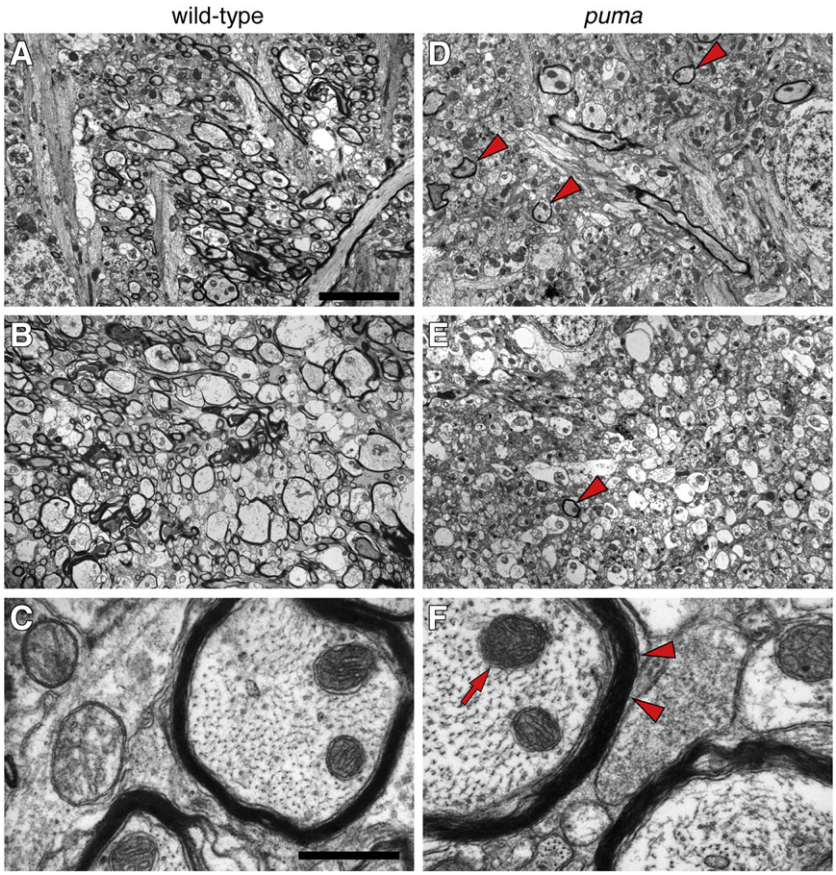

Fig. 7. Reduced myelination in *puma* mutant brains revealed by transmission electron microscopy. (A–C) Representative regions of wild-type at low magnification (5000×, A and B) and higher magnification (60,000×, C) show numerous well-myelinated axon tracts. (D–F) Corresponding regions and magnifications in *puma* reveal far fewer myelinated axon tracts (arrowheads in D and E) though layering of individual myelin sheaths that are present is indistinguishable from wild-type (arrowheads in F; arrow, mitochondrion). Scale bars: in A, 5 μm, for A, B, D, E; in C, 500 nm for C, F.

Parichy et al., 2003). Positional cloning further indicated that these defects result from a mutation in the alpha tubulin-encoding locus, *tuba8l3a*. These findings have implications for our understanding of normal myelination processes, and also identify the *puma* mutant as a valuable model in which to study dysmyelination phenotypes as well as strategies for promoting remyelination in the adult.

Several lines of evidence support our conclusion that the *puma* mutation is allelic to *tuba8l3a*. First, high-resolution mapping identified a critical genetic interval containing only two tubulin loci. Second, we identified a non-conservative missense substitution unique to the mutagenized haplotype of *tuba8l3a*. Third, the affected residue occurs at a surface site critical for the assembly of tubulin heterodimers into microtubules (Downing and Nogales, 1999; Lowe et al., 2001). Fourth, the functional importance of the affected residue is further evidenced by the near invariance of this site phylogenetically. Fifth, analyses of an adjacent candidate gene (*dnajb2*) with a coding sequence outside the critical genetic interval failed to reveal alterations in *puma* mutants. Sixth, morpholino knockdown of *tuba8l3a* in wild-type partially phenocopied a *puma* mutant *mbp* patterning defect at 5 dpf. Seventh, morpholino knockdown of the mutant *tuba8l3a* allele in the *puma* background restored *mbp* patterning to that observed in the wild-type. These results suggest that wild-type *tuba8l3a* normally contributes to microtubule function in oligodendrocytes, whereas the asn→lys substitution we identified has antimorphic effects. From structural considerations, we speculate that mutant tuba8l3a interferes with microtubule assembly or stability, though biochemical investigations beyond the scope of this study will be needed to confirm this idea.

Our phylogenetic and synteny analyses revealed evolutionary relationships among alpha tubulin genes, and point to an expansion of these loci in teleosts, perhaps owing in part to a teleost-specific genome duplication (Froschauer et al., 2006; Schweitzer et al., 2006), but also likely resulting from duplications of individual loci. The explanations for increased complexity within the family of tubulin genes remain largely unknown but presumably reflect divergence in tissue-specific expression domains (Force et al., 1999; Hall and Cowan, 1985; Schaeren-Wiemers et al., 1995) as well as divergence of protein sequence, especially relating to the potential for different post-translational modifications (McKean et al., 2001; Raff et al., 1997; Verhey and Gaertig, 2007; Wilson and Borisy, 1997). The sequences of tuba8l3a-related tubulins do not immediately suggest differences in function as compared to other alpha tubulins and the loss of *tuba8l3a* orthologues in mouse and human suggests these loci may have been redundant. Consistent with such redundancy in zebrafish, *tuba8l3b* exhibited a unique coding sequence insertion and is expressed in a domain similar to that of *tuba8l3a* (*puma*), but more weakly, suggesting recent or incipient non-functionalization (unpublished data). Our finding of an apparent instance of gene conversion between *tuba8l3a* and *tuba8l3b*, as well as the differential duplication and loss of tubulin orthologues among species, highlights the complexity of reconstructing the evolutionary history of these genes (Khodiyar et al., 2007). Existing names and orthology assignments for some tubulin genes are at variance with the phylogenetic relationships uncovered in our analyses, suggesting that further investigation is warranted. Our observations suggest that future studies of tubulin gene evolution and the assignment of gene orthologies will need to include both phylogenetic approaches and synteny analyses.

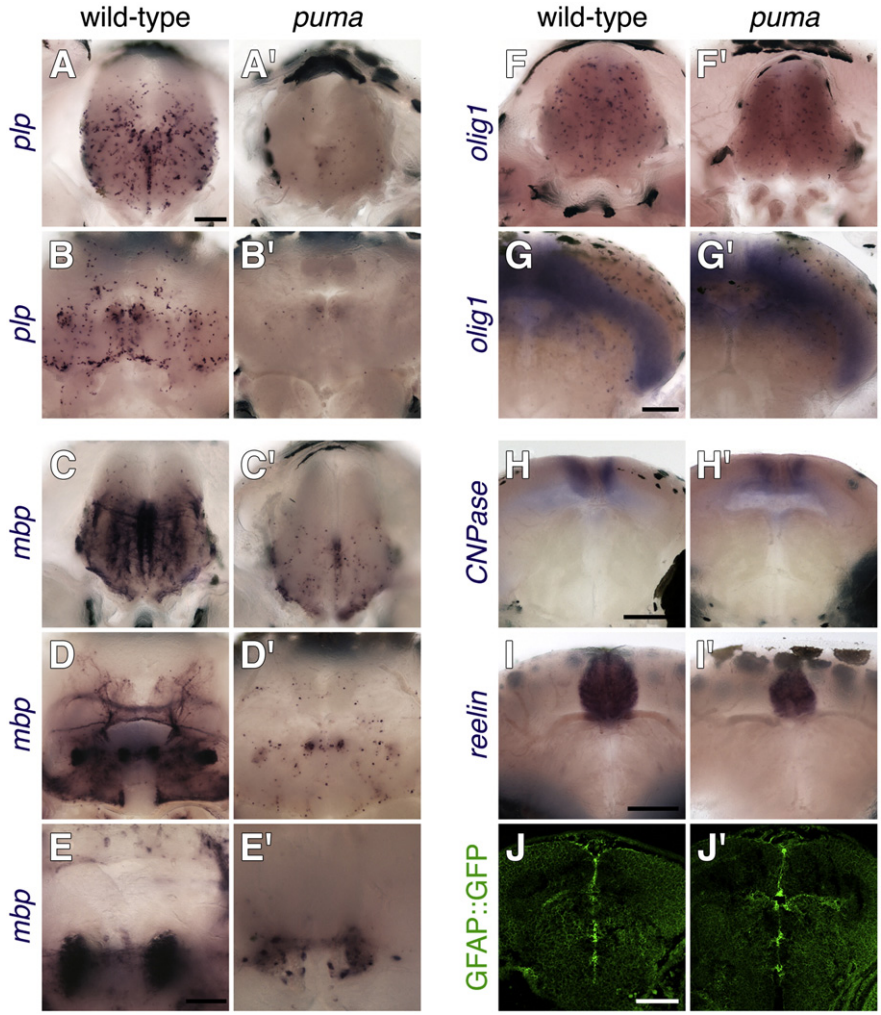

Fig. 8. Defects in oligodendrocyte number and patterning during the larval-to-adult transformation of *puma* mutants. (A, A′, B, B′) Wild-type zebrafish larvae exhibit many more *plp*+ oligodendrocytes in the brain than do *puma* mutants both during the middle larval period (A, A′; ~6.5 SSL) and the late larval period (B, B′; ~8.0 SSL). (C, C′, D, D′, E, E′) *mbp* expression also differs between wild-type and *puma* mutants during middle and later larval development (C, C′ and D, D′, respectively); a higher magnification view of different larvae is shown in E, E′. Note especially the absence of most myelinated fibers in the *puma* mutant and the concentration of *mbp* mRNA in cell bodies. (F, F′, G, G′) The early oligodendrocyte marker *olig1* does not differ in expression between genotypes at middle or later larval stages, nor do several additional markers of particular cell lineages or activities (H–J; see text for details). Scale bars: in A, 100 μm, for A, A′, B, B′, C, C′, D, D′, F, F′. In E, 40 μm for E, E′; in G, 100 μm for G, G′; in H, 100 μm for H, H′; in J, 100 μm for I, J′; in J, 100 μm for J, K′.

Microtubules have roles in numerous processes including cell shape and support, intracellular trafficking, cell division, and cell motility (Nogales, 2000; Verhey and Gaertig, 2007). In turn, the spectrum of *puma* mutant defects could reflect different microtubule functions in different cell types. In melanophores and melanocytes, for example, microtubules are required not only for cell division, but also have critical roles in the transport of melanin-containing melanosomes (Aspengren et al., 2009; Sheets et al., 2007) and, in melanoma cells in vitro, microtubules function in motility by coupling cell body advance and tail retraction (Ballestrem et al., 2000). Likewise, microtubules may influence any of several steps during myelination. For example, transport of *mbp* mRNA, several other mRNAs, and myelin-specific proteins like plp and mag, occurs in a microtubule-dependent manner (Barbarese et al., 1999; Bauer et al., 2009; Carson et al., 2001, 1997; Maier et al., 2008; Richter-Landsberg, 2008). Our finding that *puma* mutant *mbp* transcripts are abundant in oligodendrocyte cell bodies but deficient in processes suggests a reduced efficiency of trafficking. This phenotype is reminiscent of an *mbp* mRNA transport defect in zebrafish early larvae with a mutation in the kinesin motor-encoding locus *kif1b*, though these fish fail to inflate their swimbladder and are therefore not viable into later post-embryonic development (Lyons et al., 2009).

In addition to defects in *mbp* mRNA localization, our analyses using a *sox10*::GFP transgene revealed a defect in oligodendrocyte process organization, with *puma* mutant processes being more variably oriented and less compactly bundled than in wild-type. Oligodendrocyte process growth and extension require microtubules in vitro, and distinct subpopulations of microtubules, having differing stabilities, are found in different cellular regions: labile microtubules occur in fine, distal processes and branches, whereas more stable microtubules occur in main branches, and highly stable microtubules are present in the cell body (Lunn et al., 1997; Richter-Landsberg, 2008). Decreases in stability are tightly regulated and promote process extension over arborization and terminal differentiation (Lee et al., 2005; Lehotzky et al., 2009; Li et al., 2007; North et al., 2003). We speculate that mutant tuba8l3a inhibits both trafficking of myelin components and interferes with microtubule dynamics, thereby having a concomitant effect on terminal differentiation. The possibility that complex feedback mechanisms contribute to the myelination defects of *puma* mutants is further highlighted by potential roles for *mbp* in stabilizing oligodendrocyte microtubules themselves (Galiano et al., 2006). Nevertheless, we do not exclude the possibility that defects in oligodendrocyte process organization and *mbp* mRNA transport might arise secondarily from effects of tuba8l3a mutation on target axons. For example, the kif1-binding protein KBP affects axon microtubule

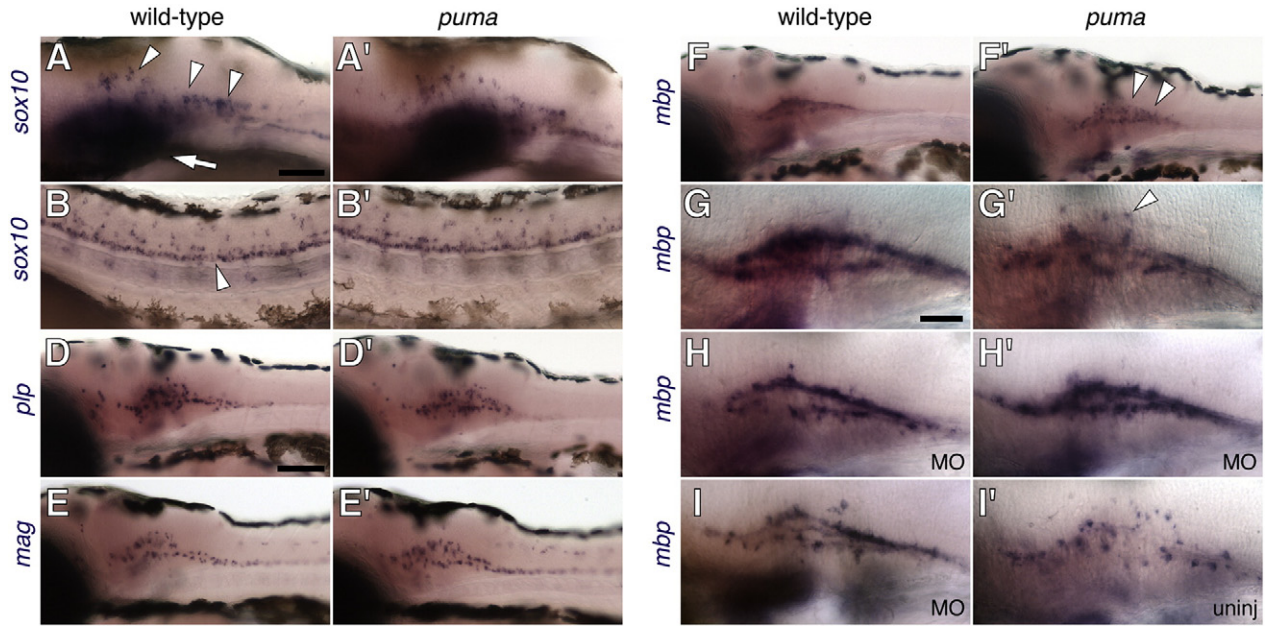

Fig. 9. Normal oligodendrocyte early differentiation but defective morphogenesis in *puma* mutant early larvae and rescue of *puma* mutant phenotype by morpholino knockdown. All panels are of 5 dpf larvae with anteriors to the left. (A, A′, B, B′) *sox10* is expressed similarly in wild-type and *puma* mutants both in the brain (A, A′) and in the spinal cord (B, B′). Arrowheads in A, dispersed *sox10*+ cells within the brain. Arrow in A, more superficial *sox10* staining within cranial ganglia. Arrowhead in B, *sox10*+ cells in the ventral spinal cord. (D, D′, E, E′) *plp* and *mag* expressions are similar between wild-type and *puma* mutants as well, with mRNA staining localizing principally to cell bodies. (F, F′) *mbp* staining, however, differs between genotypes, with wild-type *mbp*+ transcript detectable principally in oligodendrocyte processes, rather than in cell bodies, whereas in *puma* mutants, transcript is present both within processes and in cell bodies. (G, G′) Higher magnification view of different embryos, showing in wild-type compact and organized *mbp* staining in myelinating processes, but in *puma* mutants diminished staining in processes and greater staining in cell bodies (arrowhead). Although *tuba8l3a* expression in embryos was consistent with that of a maternally derived transcript, neither *mbp* mis-patterning at 5 dpf nor other phenotypes segregated as would be predicted for a maternal effect mutation (data not shown). (H) Morpholino knockdown of *tuba8l3a* results in moderate perturbations to *mbp* staining in wild-type larvae. (H′) In contrast, knockdown of *tuba8l3a* in *puma* mutants restores a wild-type pattern of *mbp* staining. (I) Partial disruption of *mbp* staining in another wild-type morphant. (I′) An uninjected *puma* mutant larva from the same clutch as the individual in H′, stained for the same duration. Morpholino dosages in H, H′, I: 0.5 ng tuba8l3a-tb1; similar results were observed with tuba8l3a-tb2 (data not shown). Scale bars: in A, 60 μm for A, A′, B, B′; in D, 100 μm for D, D′, E, E′, F, F′; in G, 40 μm for G, G′, H, H′, I, I′.

architecture, outgrowth and maintenance, and KBP mutants exhibit concomitant myelination defects (Lyons et al., 2008). Although development of the lateral line nerve (Parichy et al., 2003) and the general architecture of the CNS appear normal in *puma* mutants, defects in neuronal organization or axon outgrowth may yet be identified.

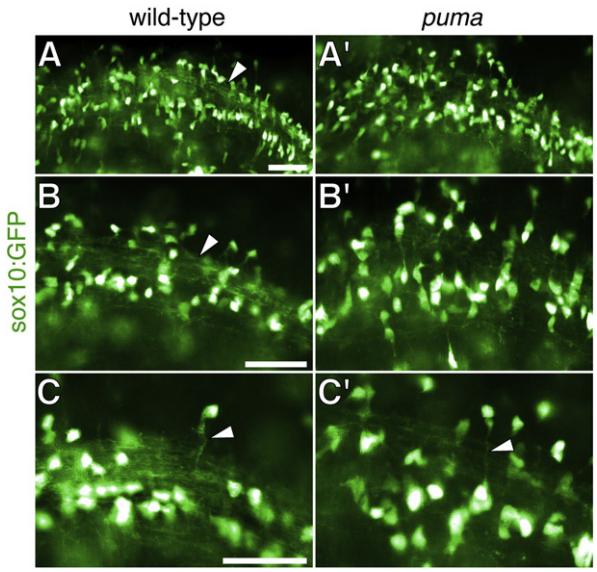

Fig. 10. Defects in oligodendrocyte patterning and myelination in *puma* mutant early larvae. (A–C) *sox10*:GFP transgene reveals oligodendrocyte cell bodies and processes, that are more disorganized in *puma* mutants than in wild-type at 5 dpf. Cell bodies are deliberately overexposed (shown here in white) to reveal fainter processes. (A, A′) Low magnification showing the orderly array of myelinating processes in wild-type (arrow), and more disorganized processes in *puma* mutants. (B, B′) Higher magnification of different individuals. (C, C′) Relatively long processes are observed in both wild-type and *puma* mutants (arrowheads). Scale bars: in A, 40 μm for A, A′; in 40 μm for B, B′; in C, 40 μm for C, C′.

Our finding of some normally myelinated axon bundles in both adult CNS and larval PNS (data not shown) of *puma* mutants indicates that some oligodendrocytes and Schwann cells can undergo an apparently normal process of myelination if they escape presumptive antimorphic effects of mutant tuba8l3a on trafficking or process organization. Effective interactions with target axons presumably allow the persistence of these cells into the adult, whereas other cells that fail to ensheath axons likely die during later larval development, or fail to differentiate fully (Simons and Trajkovic, 2006). Consistent with the idea that most oligodendrocytes die or fail to complete terminal differentiation in *puma* mutants were the gross deficiency of *plp*+ oligodendrocytes during the larval-to-adult transformation as well as the reduced *plp* staining in residual oligodendrocytes, as compared to wild-type.

An intriguing aspect of our study concerns the temporal development of *puma* mutant phenotypes. We identified abundant, spatially widespread *tuba8l3a* mRNA in early embryos and observed a gradual reduction of staining until 48 hpf, when transcripts had become undetectable by in situ hybridization. Defects in *mbp* expression and oligodendrocyte behavior first detectable at 4–5 dpf may thus reflect continuing low levels of transcription, or mutant protein perduring from earlier stages. Either possibility, as well as the different effects of knockdown in wild-type and *puma* mutants, suggests a marked sensitivity of the affected processes to perturbations of tuba8l3a dosage. During later development, we found *tuba8l3a* transcript in the post-embryonic CNS, raising the possibility of roles in later oligodendrocyte development and myelination. Nevertheless, our analyses do not yet allow us to distinguish between late and early effects of *tuba8l3a* mutation on late larval and adult myelination. For the craniofacial skeleton, we have been unable to detect differences in early patterning that might explain the adult phenotype, though sex differences in

phenotypic severity raise the possibility that hormonal factors may interact with earlier, subtle defects in cellular patterning. Precedent for early gene activities causing defects detectable only much later in the adult comes from analyses of an *erbb3b* mutant, in which adult-specific defects in neural crest-derived pigment cells result from a critical period for gene activity between 18 and 22 hpf; the same might be true for neural crest-derived Schwann cells of *puma* mutants (Budi et al., 2008). We showed previously that adult pigment pattern defects in *puma* mutants result from effects of the mutation during the larval-to-adult transformation and possibly during embryogenesis (Parichy and Turner, 2003; Parichy et al., 2003). These critical period analyses were possible owing to a temperature-sensitivity of the *puma* mutant melanophore defect that allowed for temperature shift experiments. Nevertheless, we have yet to detect temperature-dependent differences in the severity of myelination defects, so far precluding similar analyses of oligodendrocyte and Schwann cell development.

Our study identifies and characterizes a new model for studying processes of myelination as well as microtubule functions both in the embryo and in the adult. Because of their viability, we envisage that *puma* mutants should be especially useful for analyses of remyelination during post-embryonic development. Finally, further analyses of the *puma* mutant should allow testing for the presence of temporally and genetically distinct populations of glia and their precursors. For example, analyses of *puma* mutant pigment pattern defects have already been useful in distinguishing the functions and sources of temporally distinct embryonic and post-embryonic populations of melanophores (Parichy, 2006; Parichy and Turner, 2003; Parichy et al., 2003). That Schwann cells appear to develop normally in the embryo but are lost during the larval-to-adult transformation raises the possibility that *puma* mutants specifically lack a late-arising subpopulation of these cells, as is the case for melanophores. Likewise, temporally and genetically distinct populations of oligodendrocytes have been identified in other organisms (Kessaris et al., 2006), and further analyses of *puma* mutants should be useful in characterizing such populations in zebrafish, as well as the genetic and endocrine factors required for their development and maintenance.

Supplementary materials related to this article can be found online at doi:10.1016/j.ydbio.2010.07.035.

Acknowledgments

Thanks to J. Turner and M. Mills for help with genetic mapping, L. Patterson and D. Bourgin for quantitative PCR and sequencing of *dnajb2*, respectively, S. Lara and S. MacFarlane for assistance with TEM, V. Soza, R. Miller, and D. Yang for discussions about Bayesian phylogenetic methods, M. Lang for assistance with examinations of embryonic craniofacial morphology, and other members of the Parichy lab for help with fish rearing. PAC sequencing and assembly was generously provided by Y. Zhou and M. Jacobs of the UW Genome Center.

References

Aspengren, S., Hedberg, D., Skold, H.N., Wallin, M., 2009. New insights into melanosome transport in vertebrate pigment cells. Int. Rev. Cell Mol. Biol. 272, 245–302.
Ballestrem, C., Wehrle-Haller, B., Hinz, B., Imhof, B.A., 2000. Actin-dependent lamellipodia formation and microtubule-dependent tail retraction control-directed cell migration. Mol. Biol. Cell 11, 2999–3012.
Barbarese, E., Brumwell, C., Kwon, S., Cui, H., Carson, J.H., 1999. RNA on the road to myelin. J. Neurocytol. 28, 263–270.
Bauer, N.G., Richter-Landsberg, C., Ffrench-Constant, C., 2009. Role of the oligodendroglial cytoskeleton in differentiation and myelination. Glia 57, 1691–1705.
Baumann, N., Pham-Dinh, D., 2001. Biology of oligodendrocyte and myelin in the mammalian central nervous system. Physiol. Rev. 81, 871–927.
Benarroch, E.E., 2009. Oligodendrocytes: susceptibility to injury and involvement in neurologic disease. Neurology 72, 1779–1785.
Berger, P., Niemann, A., Suter, U., 2006. Schwann cells and the pathogenesis of inherited motor and sensory neuropathies (Charcot–Marie–Tooth disease). Glia 54, 243–257.
Buckley, C.E., Goldsmith, P., Franklin, R.J., 2008. Zebrafish myelination: a transparent model for remyelination? Dis. Model. Mech. 1, 221–228.
Budi, E.H., Patterson, L.B., Parichy, D.M., 2008. Embryonic requirements for ErbB signaling in neural crest development and adult pigment pattern formation. Development 135, 2603–2614.
Carson, J.H., Worboys, K., Ainger, K., Barbarese, E., 1997. Translocation of myelin basic protein mRNA in oligodendrocytes requires microtubules and kinesin. Cell Motil. Cytoskeleton 38, 318–328.
Carson, J.H., Cui, H., Krueger, W., Schlepchenko, B., Brumwell, C., Barbarese, E., 2001. RNA trafficking in oligodendrocytes. Results Probl. Cell Differ. 34, 69–81.
Chandran, S., Hunt, D., Joannides, A., Zhao, C., Compston, A., Franklin, R.J., 2008. Myelin repair: the role of stem and precursor cells in multiple sclerosis. Philos. Trans. R. Soc. Lond. B Biol. Sci. 363, 171–183.
Downing, K.H., Nogales, E., 1999. Crystallographic structure of tubulin: implications for dynamics and drug binding. Cell Struct. Funct. 24, 269–275.
Dubois-Dalcq, M., Williams, A., Stadelmann, C., Stankoff, B., Zalc, B., Lubetzki, C., 2008. From fish to man: understanding endogenous remyelination in central nervous system demyelinating diseases. Brain 131, 1686–1700.
Dutton, K.A., Pauliny, A., Lopes, S.S., Elworthy, S., Carney, T.J., Rauch, J., Geisler, R., Haffter, P., Kelsh, R.N., 2001. Zebrafish colourless encodes sox10 and specifies non-ectomesenchymal neural crest fates. Development 128, 4113–4125.
Felsenstein, J., 1989. PHYLIP — Phylogeny Inference Package (Version 3.2). Cladistics 5, 164–166.
Force, A., Lynch, M., Pickett, F.B., Amores, A., Yan, Y.L., Postlethwait, J., 1999. Preservation of duplicate genes by complementary, degenerative mutations. Genetics 151, 1531–1545.
Franklin, R.J., Ffrench-Constant, C., 2008. Remyelination in the CNS: from biology to therapy. Nat. Rev. Neurosci. 9, 839–855.
Froschauer, A., Braasch, I., Volff, J.N., 2006. Fish genomes, comparative genomics and vertebrate evolution. Curr. Genomics 7, 43–57.
Galiano, M.R., Andrieux, A., Deloulme, J.C., Bosc, C., Schweitzer, A., Job, D., Hallak, M.E., 2006. Myelin basic protein functions as a microtubule stabilizing protein in differentiated oligodendrocytes. J. Neurosci. Res. 84, 534–541.
Hall, J.L., Cowan, N.J., 1985. Structural features and restricted expression of a human alpha-tubulin gene. Nucleic Acids Res. 13, 207–223.
Hardy, R.J., 1998. Molecular defects in the dysmyelinating mutant quaking. J. Neurosci. Res. 51, 417–422.
Huelsenbeck, J.P., Ronquist, F., 2001. MRBAYES: Bayesian inference of phylogeny. Bioinformatics 17, 754–755.
Inoue, K., 2005. PLP1-related inherited dysmyelinating disorders: Pelizaeus–Merzbacher disease and spastic paraplegia type 2. Neurogenetics 6, 1–16.
Ivanova, A., Nakahira, E., Kagawa, T., Oba, A., Wada, T., Takebayashi, H., Spassky, N., Levine, J., Zalc, B., Ikenaka, K., 2003. Evidence for a second wave of oligodendrogenesis in the postnatal cerebral cortex of the mouse. J. Neurosci. Res. 73, 581–592.
Jaglin, X.H., Poirier, K., Saillour, Y., Buhler, E., Tian, G., Bahi-Buisson, N., Fallet-Bianco, C., Phan-Dinh-Tuy, F., Kong, X.P., Bomont, P., Castelnau-Ptakhine, L., Odent, S., Loget, P., Kossorotoff, M., Snoeck, I., Plessis, G., Parent, P., Beldjord, C., Cardoso, C., Represa, A., Flint, J., Keays, D.A., Cowan, N.J., Chelly, J., 2009. Mutations in the beta-tubulin gene TUBB2B result in asymmetrical polymicrogyria. Nat. Genet. 41, 746–742.
Jessen, K.R., Mirsky, R., 2005. The origin and development of glial cells in peripheral nerves. Nat. Rev. Neurosci. 6, 671–682.
Kalani, M.Y., Cheshier, S.H., Cord, B.J., Bababeygy, S.R., Vogel, H., Weissman, I.L., Palmer, T.D., Nusse, R., 2008. Wnt-mediated self-renewal of neural stem/progenitor cells. Proc. Natl. Acad. Sci. U. S. A. 105, 16970–16975.
Keays, D.A., Tian, G., Poirier, K., Huang, G.J., Siebold, C., Cleak, J., Oliver, P.L., Fray, M., Harvey, R.J., Molnar, Z., Pinon, M.C., Dear, N., Valdar, W., Brown, S.D., Davies, K.E., Rawlins, J.N., Cowan, N.J., Nolan, P., Chelly, J., Flint, J., 2007. Mutations in alpha-tubulin cause abnormal neuronal migration in mice and lissencephaly in humans. Cell 128, 45–57.
Kessaris, N., Fogarty, M., Iannarelli, P., Grist, M., Wegner, M., Richardson, W.D., 2006. Competing waves of oligodendrocytes in the forebrain and postnatal elimination of an embryonic lineage. Nat. Neurosci. 9, 173–179.
Khodiyar, V.K., Maltais, L.J., Ruef, B.J., Sneddon, K.M., Smith, J.R., Shimoyama, M., Cabral, F., Dumontet, C., Dutcher, S.K., Harvey, R.J., Lafanechere, L., Murray, J.M., Nogales, E., Piquemal, D., Stanchi, F., Povey, S., Lovering, R.C., 2007. A revised nomenclature for the human and rodent alpha-tubulin gene family. Genomics 90, 285–289.
Kim, H., Shin, J., Kim, S., Poling, J., Park, H.C., Appel, B., 2008. Notch-regulated oligodendrocyte specification from radial glia in the spinal cord of zebrafish embryos. Dev. Dyn. 237, 2081–2089.
Kimmel, C.B., Ballard, W.W., Kimmel, S.R., Ullmann, B., Schilling, T.F., 1995. Stages of embryonic development of the zebrafish. Dev. Dyn. 203, 253–310.
Kirby, B.B., Takada, N., Latimer, A.J., Shin, J., Carney, T.J., Kelsh, R.N., Appel, B., 2006. In vivo time-lapse imaging shows dynamic oligodendrocyte progenitor behavior during zebrafish development. Nat. Neurosci. 9, 1506–1511.
Le Douarin, N.M., 1999. The Neural Crest. Cambride University Press, Cambridge.
Lee, J., Gravel, M., Zhang, R., Thibault, P., Braun, P.E., 2005. Process outgrowth in oligodendrocytes is mediated by CNP, a novel microtubule assembly myelin protein. J. Cell Biol. 170, 661–673.
Lehotzky, A., Lau, P., Tokesi, N., Muja, N., Hudson, L.D., Ovadi, J., 2009. Tubulin polymerization-promoting protein (TPPP/p25) is critical for oligodendrocyte differentiation. Glia 58, 157–168.
Li, W., Zhang, B., Tang, J., Cao, Q., Wu, Y., Wu, C., Guo, J., Ling, E.A., Liang, F., 2007. Sirtuin 2, a mammalian homolog of yeast silent information regulator-2 longevity regulator, is an oligodendroglial protein that decelerates cell differentiation through deacetylating alpha-tubulin. J. Neurosci. 27, 2606–2616.
Lowe, J., Li, H., Downing, K.H., Nogales, E., 2001. Refined structure of alpha beta-tubulin at 3.5 A resolution. J. Mol. Biol. 313, 1045–1057.

Lunn, K.F., Baas, P.W., Duncan, I.D., 1997. Microtubule organization and stability in the oligodendrocyte. J. Neurosci. 17, 4921–4932.
Lyons, D.A., Pogoda, H.M., Voas, M.G., Woods, I.G., Diamond, B., Nix, R., Arana, N., Jacobs, J., Talbot, W.S., 2005. erbb3 and erbb2 are essential for Schwann cell migration and myelination in zebrafish. Curr. Biol. 15, 513–524.
Lyons, D.A., Naylor, S.G., Mercurio, S., Dominguez, C., Talbot, W.S., 2008. KBP is essential for axonal structure, outgrowth and maintenance in zebrafish, providing insight into the cellular basis of Goldberg–Shprintzen syndrome. Development 135, 599–608.
Lyons, D.A., Naylor, S.G., Scholze, A., Talbot, W.S., 2009. Kif1b is essential for mRNA localization in oligodendrocytes and development of myelinated axons. Nat. Genet. 41, 854–858.
Maier, O., Hoekstra, D., Baron, W., 2008. Polarity development in oligodendrocytes: sorting and trafficking of myelin components. J. Mol. Neurosci. 35, 35–53.
McKean, P.G., Vaughan, S., Gull, K., 2001. The extended tubulin superfamily. J. Cell Sci. 114, 2723–2733.
McTigue, D.M., Tripathi, R.B., 2008. The life, death, and replacement of oligodendrocytes in the adult CNS. J. Neurochem. 107, 1–19.
Menn, B., Garcia-Verdugo, J.M., Yaschine, C., Gonzalez-Perez, O., Rowitch, D., Alvarez-Buylla, A., 2006. Origin of oligodendrocytes in the subventricular zone of the adult brain. J. Neurosci. 26, 7907–7918.
Monk, K.R., Talbot, W.S., 2009. Genetic dissection of myelinated axons in zebrafish. Curr. Opin. Neurobiol. 19, 486–490.
Monk, K.R., Naylor, S.G., Glenn, T.D., Mercurio, S., Perlin, J.R., Dominguez, C., Moens, C.B., Talbot, W.S., 2009. A G protein-coupled receptor is essential for Schwann cells to initiate myelination. Science 325, 1402–1405.
Nave, K.A., Trapp, B.D., 2008. Axon-glial signaling and the glial support of axon function. Annu. Rev. Neurosci. 31, 535–561.
Ndubaku, U., de Bellard, M.E., 2008. Glial cells: old cells with new twists. Acta Histochem. 110, 182–195.
Nguyen, L., Borgs, L., Vandenbosch, R., Mangin, J.M., Beukelaers, P., Moonen, G., Gallo, V., Malgrange, B., Belachew, S., 2006. The Yin and Yang of cell cycle progression and differentiation in the oligodendroglial lineage. Ment. Retard. Dev. Disabil. Res. Rev. 12, 85–96.
Nogales, E., 2000. Structural insights into microtubule function. Annu. Rev. Biochem. 69, 277–302.
Nogales, E., Downing, K.H., Amos, L.A., Lowe, J., 1998a. Tubulin and FtsZ form a distinct family of GTPases. Nat. Struct. Biol. 5, 451–458.
Nogales, E., Wolf, S.G., Downing, K.H., 1998b. Structure of the alpha beta tubulin dimer by electron crystallography. Nature 391, 199–203.
North, B.J., Marshall, B.L., Borra, M.T., Denu, J.M., Verdin, E., 2003. The human Sir2 ortholog, SIRT2, is an NAD+-dependent tubulin deacetylase. Mol. Cell 11, 437–444.
Parichy, D.M., 2006. Evolution of Danio pigment pattern development. Heredity 97, 200–210.
Parichy, D.M., Turner, J.M., 2003. Zebrafish puma mutant decouples pigment pattern and somatic metamorphosis. Dev. Biol. 256, 242–257.
Parichy, D.M., Turner, J.M., Parker, N.B., 2003. Essential role for puma in development of postembryonic neural crest-derived cell lineages in zebrafish. Dev. Biol. 256, 221–241.
Parichy, D. M., Elizondo, M. R., Mills, M. G., Gordon, T. N., Engeszer, R. E., 2009. Normal table of zebrafish post-embryonic development: staging by externally visible anatomy of the living fish. Dev. Dyn. 238, 2975–3015.
Pogoda, H.M., Sternheim, N., Lyons, D.A., Diamond, B., Hawkins, T.A., Woods, I.G., Bhatt, D.H., Franzini-Armstrong, C., Dominguez, C., Arana, N., Jacobs, J., Nix, R., Fetcho, J.R., Talbot, W.S., 2006. A genetic screen identifies genes essential for development of myelinated axons in zebrafish. Dev. Biol. 298, 118–131.
Poirier, K., Keays, D.A., Francis, F., Saillour, Y., Bahi, N., Manouvrier, S., Fallet-Bianco, C., Pasquier, L., Toutain, A., Tuy, F.P., Bienvenu, T., Joriot, S., Odent, S., Ville, D., Desguerre, I., Goldenberg, A., Moutard, M.L., Fryns, J.P., van Esch, H., Harvey, R.J., Siebold, C., Flint, J., Beldjord, C., Chelly, J., 2007. Large spectrum of lissencephaly and pachygyria phenotypes resulting from de novo missense mutations in tubulin alpha 1A (TUBA1A). Hum. Mutat. 28, 1055–1064.
Potthoff, T., 1984. Clearing and staining techniques. In: Moser, H.G., Richards, W.J., Cohen, D.M., Fahay, M.P., Kendall Jr., A.W., Richardson, S.L. (Eds.), Ontogeny and systematics of fishes (based on an international symposium dedicated to the memory of Elbert Halvor Ahlstrom). : Special Publication 1, American Society of Ichthyologists and Herpetologists. Allen Press, Lawrence, KS, pp. 35–37.
Raff, E.C., Fackenthal, J.D., Hutchens, J.A., Hoyle, H.D., Turner, F.R., 1997. Microtubule architecture specified by a beta-tubulin isoform. Science 275, 70–73.
Readhead, C., Hood, L., 1990. The dysmyelinating mouse mutations shiverer (shi) and myelin deficient (shimld). Behav. Genet. 20, 213–234.
Richter-Landsberg, C., 2008. The cytoskeleton in oligodendrocytes. Microtubule dynamics in health and disease. J. Mol. Neurosci. 35, 55–63.
Roach, A., Takahashi, N., Pravtcheva, D., Ruddle, F., Hood, L., 1985. Chromosomal mapping of mouse myelin basic protein gene and structure and transcription of the partially deleted gene in shiverer mutant mice. Cell 42, 149–155.
Schaeren-Wiemers, N., Schaefer, C., Valenzuela, D.M., Yancopoulos, G.D., Schwab, M.E., 1995. Identification of new oligodendrocyte- and myelin-specific genes by a differential screening approach. J. Neurochem. 65, 10–22.
Scherer, S.S., Wrabetz, L., 2008. Molecular mechanisms of inherited demyelinating neuropathies. Glia 56, 1578–1589.
Schmued, L., Bowyer, J., Cozart, M., Heard, D., Binienda, Z., Paule, M., 2008. Introducing Black-Gold II, a highly soluble gold phosphate complex with several unique advantages for the histochemical localization of myelin. Brain Res. 1229, 210–217.
Schweitzer, J., Becker, T., Schachner, M., Nave, K.A., Werner, H., 2006. Evolution of myelin proteolipid proteins: gene duplication in teleosts and expression pattern divergence. Mol. Cell. Neurosci. 31, 161–177.
Sheets, L., Ransom, D.G., Mellgren, E.M., Johnson, S.L., Schnapp, B.J., 2007. Zebrafish melanophilin facilitates melanosome dispersion by regulating dynein. Curr. Biol. 17, 1721–1734.
Simons, M., Trajkovic, K., 2006. Neuron-glia communication in the control of oligodendrocyte function and myelin biogenesis. J. Cell Sci. 119, 4381–4389.
Simons, M., Trotter, J., 2007. Wrapping it up: the cell biology of myelination. Curr. Opin. Neurobiol. 17, 533–540.
Tian, G., Kong, X.P., Jaglin, X.H., Chelly, J., Keays, D., Cowan, N.J., 2008. A pachygyria-causing alpha-tubulin mutation results in inefficient cycling with CCT and a deficient interaction with TBCB. Mol. Biol. Cell 19, 1152–1161.
Verhey, K.J., Gaertig, J., 2007. The tubulin code. Cell Cycle 6, 2152–2160.
Voas, M.G., Lyons, D.A., Naylor, S.G., Arana, N., Rasband, M.N., Talbot, W.S., 2007. alphaII-spectrin is essential for assembly of the nodes of Ranvier in myelinated axons. Curr. Biol. 17, 562–568.
Wenger, D.A., Rafi, M.A., Luzi, P., Datto, J., Costantino-Ceccarini, E., 2000. Krabbe disease: genetic aspects and progress toward therapy. Mol. Genet. Metab. 70, 1–9.
Wenning, G.K., Stefanova, N., Jellinger, K.A., Poewe, W., Schlossmacher, M.G., 2008. Multiple system atrophy: a primary oligodendrogliopathy. Ann. Neurol. 64, 239–246.
Wilson, P.G., Borisy, G.G., 1997. Evolution of the multi-tubulin hypothesis. Bioessays 19, 451–454.
Woodhoo, A., Sommer, L., 2008. Development of the Schwann cell lineage: from the neural crest to the myelinated nerve. Glia 56, 1481–1490.
Woods, I.G., Lyons, D.A., Voas, M.G., Pogoda, H.M., Talbot, W.S., 2006. nsf is essential for organization of myelinated axons in zebrafish. Curr. Biol. 16, 636–648.
Woodward, K.J., 2008. The molecular and cellular defects underlying Pelizaeus–Merzbacher disease. Expert Rev. Mol. Med. 10, e14.
Zeis, T., Schaeren-Wiemers, N., 2008. Lame ducks or fierce creatures? The role of oligodendrocytes in multiple sclerosis. J. Mol. Neurosci. 35, 91–100.